Applied Energy 383 (2025) 125306

Contents lists available at ScienceDirect

Applied Energy

journal homepage: www.elsevier.com/locate/apenergy

Thermal performance analysis of a heat pump-based energy system to meet heating and cooling demand of residential buildings

Arslan Saleem *, Carlos E. Ugalde-Loo

School of Engineering, Cardiff University, Queen's Buildings, The Parade, Cardiff CF24 3AA, Wales, UK

HIGHLIGHTS

- A dynamic model of a heat pump-based energy supply technology is developed.
- The multi-zone modelling approach is adopted to simulate a terraced house in Wales.
- Internal heat gain due to appliances, lighting, and occupancy schedule is modelled.
- The heat pump system uses ~1.6 times less energy annually compared to a gas boiler.
- Internal heat gains affect the heat pump's annual energy consumption by 15.5 %.

GRAPHICAL ABSTRACT

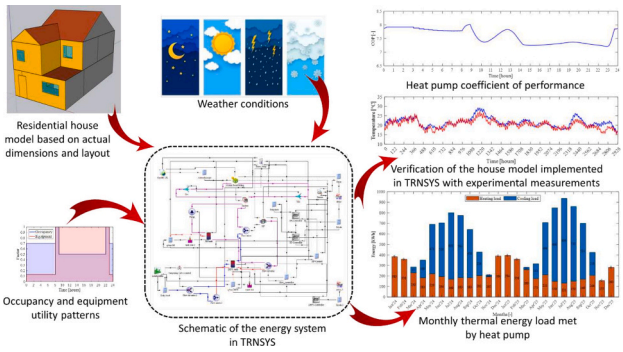

ARTICLE INFO

Keywords:
Reversible heat pump
Gas boiler
Thermal performance
TRNSYS
Coefficient of performance

ABSTRACT

The building sector significantly impacts greenhouse gas emissions, making decarbonisation of heating and cooling essential for achieving carbon neutrality. Replacing conventional fossil fuel technologies with low-carbon alternatives like reversible heat pumps (HPs), alongside integrating thermal energy storage systems, can provide flexibility by reducing thermal demand during peak hours—which could also be reflected in economic savings. In view of this, the detailed dynamic model of an energy system based on a reversible HP integrated with thermal stores is presented in this paper. The adopted configuration has been designed to meet not only heat demand during cold months, but also cooling demand over summer, which is expected to increase in future years according to climate projections. A multi-zone modelling approach was employed to simulate a residential building. Internal heat gains due to appliances, lighting, and occupancy schedules were incorporated in the model to accurately represent the zonal temperature level control in the thermal envelope. The performance of the energy system utilising the reversible HP was compared to when a gas boiler is used, demonstrating the capabilities of low-carbon technologies to meet thermal demand during different seasons of the year. Moreover, the performance of HP-based system under extreme weather conditions was evaluated. The HP configuration consumed 1.15–2.34 times less monthly energy to meet the thermal needs compared to the boiler-based system. The inclusion of internal heat gains showed a considerable effect, with a monthly energy consumption increment of up to 63.5 % observed for the HP-based energy system.

* Corresponding author.
E-mail address: SaleemA7@cardiff.ac.uk (A. Saleem).

https://doi.org/10.1016/j.apenergy.2025.125306
Received 16 May 2024; Received in revised form 20 December 2024; Accepted 3 January 2025

1. Introduction

The building sector accounts for 30 % of the global final energy consumption and 27 % of the total energy sector emissions [1]. Thus, over the past few decades, the building stock has been recognised as a crucial area for reducing energy consumption and transitioning to a low-carbon energy supply [2]. This in turn has led to a growing body of literature dedicated to developing retrofit strategies for buildings to curtail energy consumption [3]. These strategies encompass a range of approaches, including enhancing thermal efficiency of the building fabric [4], implementing building-integrated passive systems [5], and integrating technologies such as heat pumps (HPs) [6] and combined heat and power systems [7]. However, recent research findings highlight an emerging need to optimise the performance of technical systems alongside improvements in building fabric [8]. Furthermore, the integration of renewable energy sources [9] into the electricity grid, particularly when combined with the electrification of space heating in buildings, has emerged as a prospective pathway that numerous countries are considering to achieve decarbonisation goals [10].

HP systems can be integrated with renewable energy sources like the air, ground, groundwater, or solar as heat sources or heat sinks to enhance energy efficiency [11]. While HP technologies are being incorporated in new constructions, particularly in low-temperature heating applications such as radiant floor heating, their retrofitting into existing buildings poses challenges in terms of space limitation and cost-effectiveness [12]. The elevated temperature requirements of conventional heating systems remain a primary technical barrier hindering the wider adoption of HPs, particularly in multi-family buildings. For instance, field studies reported in [13] involving nearly 250 HP systems revealed that retrofitted HP systems consume, on average, 20 % more electricity compared to their counterparts in new constructions. Likewise, heat source types and supply temperatures have been identified as crucial determinants for achieving efficient system operation in retrofit HP systems [14].

Central to the effectiveness of HP systems is the space heating emission system, which directly influences the required temperature levels [15]. Emphasis has been placed on hydronic radiator heating systems, as these are commonly found in existing European buildings. These radiator systems are frequently over-dimensioned, offering potential for operation at lower heating temperatures without compromising comfort levels [16]. Rather than a complete system overhaul, a targeted approach involving the replacement of bottleneck radiators responsible for demanding maximum system temperatures has shown promise. Successful implementation of such strategies requires meticulous hydronic balancing to ensure uniform flow distribution and, consequently, lower temperatures.

In the context of low-temperature district heating networks, radiator heating systems in renovated Danish buildings were explored in [17]. Through selective radiator replacements, these systems successfully achieve reduced nominal heating temperatures. Similar findings were highlighted in [18], where a comprehensive survey of radiator systems within a Danish district heating network was reported—further underscoring the importance of tailored analysis based on factors such as radiator capacity, building age, renovation status, and nominal heating load.

A multitude of studies have delved into optimising HP performance in multi-family buildings. Reference [19] investigated the combination of radiator systems and radiant floor heating to achieve lower nominal supply and return temperatures in existing Finnish apartment buildings. Reference [20] compared the energy efficiency of ground-coupled HPs connected to radiators and radiant floor heating systems, demonstrating the viability of radiator systems for well-insulated structures. Simulation results of HP systems with different heat sources to meet the energy demand for multi-family buildings in Geneva, Switzerland, were reported in [21]. The energy demand of a typical building was calculated through rescaling of the reference meteorological year and assumptions were made regarding the available roof and ground area for solar and geothermal energy sources. Other references available in the literature have examined the influence of low-temperature heating systems on heat distribution and emission losses, showcasing the potential for improved performance [15,22,23].

Control strategies aimed at reducing temperatures in radiator heating systems have been also explored [24–26]. These include adaptive heating curves for low-temperature district heating, algorithms optimising supply temperatures, and dynamic optimisation of radiator temperature differences based on real-time heat demand.

In [11] a newly developed TRNSYS element (Type) to simulate a reversible water-to-water HP with different configurations and refrigerant fluids was presented. This element was employed to investigate the operation of a ground-source HP capable of providing space heating and space cooling to a historic building. However, hot water production was not modelled in the study. In reference [27], a novel zoned group control method based on a resistor–capacitor model predictive control (RC-MPC) scheme was proposed to achieve precise and stable indoor room temperature for a space heating building using the software package IDA ICE. In a similar vein, different energy system scenarios consisting of electric and hybrid HPs were investigated for a range of different building retrofit measures in [28] utilising IES-VE. Another interesting reference is [29], where a dynamic simulation for performance evaluation of an energy system consisting of a positive energy building was conducted using TRNSYS. These recent references focused on space heating and domestic hot water supply, ignoring the space cooling demand.

Recently, reference [30] investigated energy system configurations simultaneously using thermal energy storage (TES) and electrical energy storage (EES) units to increase the self-sufficiency of energy demand for heating, cooling, and hot water production. A radiant floor system was used for space heating and cooling and four different configurations of TES and EES were modelled. In [31], simulations using TRNSYS were performed for an existing energy-efficient single-family residential building, with floor heating and mechanical ventilation, located in north-eastern Poland. In the study, the impact of setting the heating curve on reducing gas consumption in the residential building while ensuring thermal comfort was assessed.

Other references have also looked into the effect of solar-assisted HP technologies. In [32], a solar-assisted ground-source HP system was modelled. This system was installed in a low-rise residential apartment building located in Erzurum, Turkey. The performance of the solar-assisted system was assessed to evaluate its potential for net-zero energy buildings. In the study, while space heating and domestic hot water production was modelled, space cooling was not considered. In [33] two heating schemes for a single rural residential building in Harbin, China, were designed and simulated. One was based on a ground-source HP system and the other one on a solar ground-source HP system. However, space cooling and hot water demand were not modelled as part of the study.

The existing research discussed in the previous paragraphs primarily focuses on low-temperature space heating to enhance the energy efficiency of HP systems, often neglecting the high temperature requirements for domestic hot water (DHW). Furthermore, few references assess the thermal response of building models using real weather data or actual operating conditions of the HP system, particularly in the UK. Within the UK context specifically, most of the available research has centred on heating demand, overlooking cooling needs despite rising summer temperatures and the more frequent and severe heatwaves. Cooling has received limited attention [34], even though National Grid, owner of the national electricity transmission system in England and Wales, anticipates an additional 19–39 GW to peak electricity demand by 2050 due to increased air-conditioning usage [35]. This oversight persists despite growing concerns about overheating in UK homes. Consideration of domestic cooling demand in the UK research and policy landscape, supported by comprehensive data, is still lacking [36].

This paper addresses the gaps just highlighted by investigating the effect of low-carbon technologies to meet both the heating and cooling demand of a residential dwelling located in the UK. This is done using TRNSYS, a dynamic model simulator, to model a single-family home in Cardiff, Wales. To provide credibility into the modelling approach, the model incorporates real weather data and internal heat gains from occupancy, lighting, and electrical equipment. These are defined based on standard schedules informed by the Chartered Institution of Building Services Engineers (CIBSE), an international professional engineering association based in England representing building services engineers. A TES system integrated with a reversible HP is used to meet both space heating and cooling needs, as well as year-round DHW demand, as opposed to other studies available in the literature which do not consider the three elements concurrently. The performance of the presented TES-HP system is compared to the performance exhibited by a conventional gas boiler, providing insights into retrofitting prospects of the presented configuration. Additionally, climate projections are utilised to evaluate the system's performance under extreme weather scenarios—a novel approach within the UK context.

2. Methodology

Dynamic modelling of the system under study was performed using TRNSYS, which is a widely adopted software package to simulate the transient behaviour of energy systems [37]. The software has a modular structure which allows the numerical modelling of a wide range of system components. The performance maps of components are based on actual data from commercially available products corresponding to different operating conditions. Moreover, TRNSYS facilitates the design and simulation of numerous system configurations which can be tailored to specific requirements and operated under various control schedules. The validity and the robustness of TRNSYS is supported by various case studies based on energy rate modelling of different buildings and temperature level modelling of heating, ventilation and air-conditioning (HVAC) systems [11,38].

A simple block diagram of the system under investigation is shown in Fig. 1, which involves detailed modelling of a residential building. The intricacy of the model was improved by incorporating building material properties, weather conditions, and internal heat gains. An energy system along with its operation control scheme based on indoor thermal comfort criteria was developed to meet heating and cooling demand of the building. The elements of the block diagram are discussed in detail in the following subsections.

2.1. The climate

The selected residential building for analysis is located in Cardiff, Wales, UK. The thermal load profile of the building was determined by accounting for prevailing climatic conditions. The historical weather data from year 2022 specific to this location were sourced from [39]. Fig. 2 shows the ambient temperature fluctuations during the adopted year (see light blue trace, with the average temperature shown with a black trace), illustrating a relatively hot climate year-round with maximum temperature reaching 32.5 °C in August. Intense periods of elevated temperatures and global horizontal irradiation (GHI, shown with a red trace) occurred from June to August (i.e. from 3650 h to 5840 h in the graph).

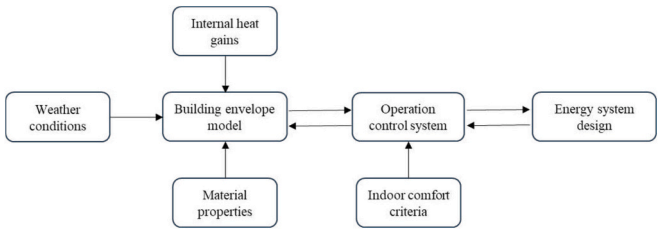

Fig. 1. Block diagram of the system under study.

2.2. Building envelope description

The residential building considered for the analysis is a three-bedroom two-storey house with a total floor area of 79 m^2 and a volume of 180 m^3. Fig. 3 shows the floor plan of the house under investigation, detailing the sizes of nine different spaces. This information was obtained from [40], where publicly available floor plans for residential homes in the UK are provided. From here onwards the spaces are referred to as zones. The building envelope was modelled using the software SketchUp. A screenshot of the envelope is shown in Fig. 4, while the thermal properties of different components (ground, roof, walls, and windows) of the envelope were defined in TRNBuild. Each component used in the building fabric is composed of a different set of materials called layers. Details of the building components along with thermophysical properties of each layer are provided in Table 1.

Building operation is defined by the ventilation system and internal gains due to occupancy, lighting systems, and electrical equipment. The average occupancy of a household in Wales is 2.4 people per household [41]; however, the design methodology developed by CIBSE for assessment of overheating risk in homes [42] was adopted in the present work. According to standard TM59 from CIBSE, a 24 h occupancy profile should be used for bedrooms. Each bedroom was considered occupied by one person during the day and two people are assumed to occupy each double bedroom during the night. The kitchen and living room were considered occupied during the day and unoccupied during night-time. In addition, the overall apartment was modelled as occupied for 24 h and no differences between weekdays and weekends were considered. All doors and windows exposed to the outdoor environment were assumed closed throughout. Only five zones in the building envelope (namely, the kitchen, living room, and three bedrooms) were considered for temperature control. For simplicity, the zones comprising the entrance area, stairs, and toilet were not selected for active temperature control due to lack of their occupancy data. Zone Sp6 is a double bedroom and Zones Sp5 and Sp7 are single bedrooms. The occupancy and equipment use pattern of each zone is shown in Fig. 5 and the internal heat gain due to occupancy, equipment, and lighting for each zone, calculated according to CIBSE standards, are shown in Table 2.

The profiles and associated loads shown in Fig. 5 are described in more detail next. According to [43], the maximum sensible heat gain is 75 W per person in living spaces, whereas the maximum latent heat gain is 55 W per person. During sleeping hours, a 30 % reduction in gains is applied [44]. Lighting energy was assumed to be proportional to floor area, with lighting loads measured in W/m^2. From 6 pm to 11 pm, a default lighting load of 2 W/m^2 was considered under the assumption that adequate daylight levels are available and that the home is energy efficient.

With regards to the equipment gains in Fig. 5, the profile and the associated loads adopted from [42] were derived from [45,46]. Details of the specific equipment are not provided in [42], but the internal gain and equipment patterns are based on the electricity consumption and appliances utility patterns gathered from surveys of UK households. It was also assumed that each bedroom in the house had the same appliances and that the heat loads from appliances are independent of floor area.

Taking into account average occupancy and the equipment profiles available in [46] and multiplying by the peak gains per appliance available in the same reference, the total gains per hour for each room shown in Table 2 were calculated.

It is relevant to highlight that CIBSE TM59 was designed to evaluate building designs for mitigating overheating risks and, thus, requires consideration of lengthy occupancy periods. In addition, building modelling assumes a constant occupancy as using a different approach

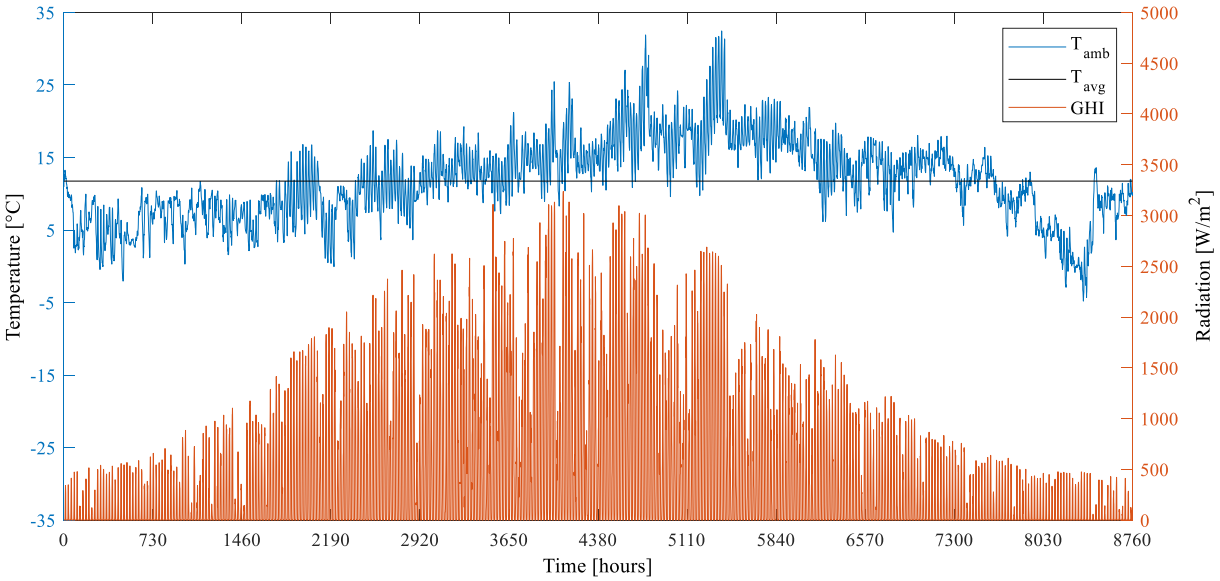

Fig. 2. Historical weather data of Cardiff, Wales, UK, for year 2022.

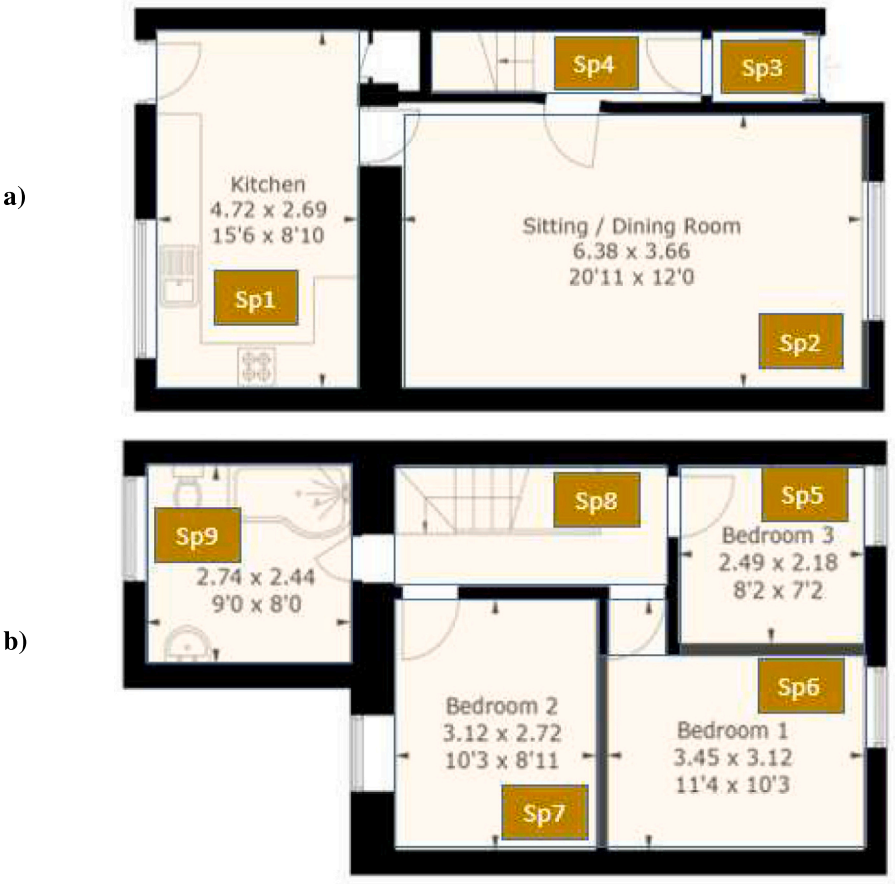

Fig. 3. Layout of the residential house [40]: a) Ground floor. b) First floor.

for overheating is considered inconsistent and confusing [42]. Given that in this paper the potential for meeting both heating and cooling demand of a residential building located in the UK is assessed, occupancy and equipment patterns based on [42] were adopted for the simulation studies reported in Section 4. However, ISO recommended profiles are also assessed in Section 4.6 to consider more realistic patterns.

2.3. Numerical model and settings

TRNSYS Simulation Studio was used for dynamic simulation of the system under study. Different components from the TRNSYS library

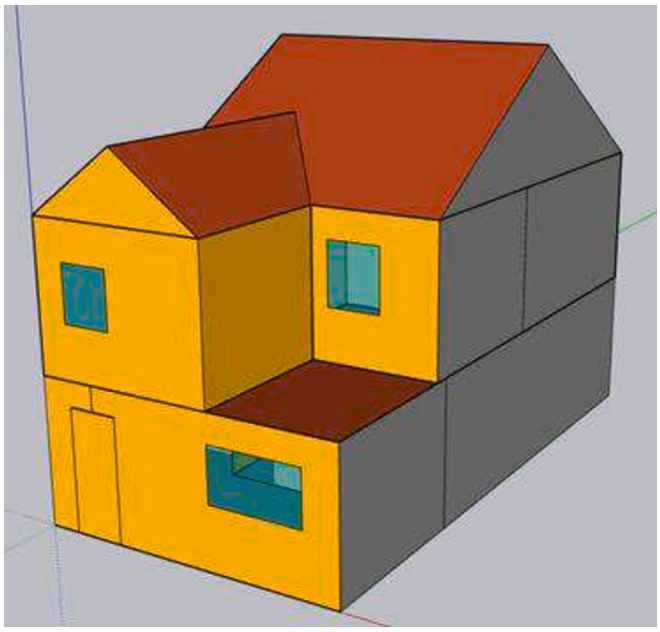

Fig. 4. Screenshot of building model developed in SketchUp.

were used to model the HVAC system. These components have a pre-assigned name with the prefix "Type". Proportional-integral (PI) controllers (Type23) were employed to regulate the operation of the energy system. Five control loops were designed in total. For a system configuration based on a gas boiler (Type700_v2a) to meet heat demand, a PI controller was implemented to regulate DHW provision and another one for space heating based on specified temperature setpoints. If an HP was used instead to meet thermal demand (for both heating and cooling), three PI-based control loops were implemented, with a similar approach as for the boiler-based system, and an additional control loop for cooling provision facilitated by the reversible operation of the HP. (Whether driven by a gas boiler or a HP, the control loop for DHW provision operates based on the water temperature of a hot water tank (HWT). This is explained later in the section.)

In the case of an HP-based energy system, the PI controller for space heating modulates the electrical power input to the HP to modify its thermal power output—thus enabling zone temperature regulation at a specified heating setpoint. A second PI controller was used in a similar manner to regulate the provision of space cooling according to a cooling setpoint. Following the guidelines from CIBSE Guide A [43], a heating setpoint of 19 °C was adopted for all five thermal zones with temperature level control. The same setpoint was used when a gas boiler was employed instead. For space cooling provision by the HP, a cooling setpoint of 23 °C was used. In the colder months, when the air temperature drops below 19 °C, the gas boiler or the HP were used to warm up the house. During the warmer months, when the air temperature exceeds 23 °C in any zone, the HP was operated in a reversible cycle to cool down the zonal space. Fig. 6 shows a flowchart describing the operation of the energy system. Key parameters of the PI controllers are summarised in Table 3. These were selected following a heuristic approach which, for the HP, ensured its smooth operation by minimising on/off cycling. Having a PI-based control scheme for both the HP and the gas boiler based energy systems enabled a fair comparison of their performance.

A water-to-water HP (Type927_v2a) was initially selected as the primary technology to meet the household's heating and cooling demand. This specific model features a single-speed compressor and accounts for the effects of air humidity. Consistent with other HP models available in the TRNSYS TESS library, the operation of Type927_v2a is determined through associated performance data. By default, HP operation is based on two activation signals taking values between 0 and 1. One signal is used to trigger the heating mode and the second one for the cooling mode. The mode of operation would be selected depending on the temperature setpoints as highlighted in the previous paragraph. Once the operating mode is established, a value above 0.5 in the triggering signal would result in the HP being activated, whereas a signal with a value below 0.5 would switch off the HP. In the literature, a multi-zone thermostat Type698 has been implemented to achieve temperature regulation in multiple zones [47]. Type698 operates by comparing the zone temperature of the thermal envelope with the setpoint temperature and can be used to prompt HP operation if its output is used as an activation signal for the HP. However, since this thermostat model only outputs values of either 0 or 1, it leads to an on-off HP operation. Such temperature regulation approach is not practical and may yield an inadequate HP utilisation.

To facilitate practical HP operation, the source code of Type927 was modified, resulting in a customised component named Type9271. This new HP block enables modulation of the HP thermal power output by adjusting its electrical power input based on input values between 0 and 1. A value of 0 would indicate the HP is switched off, a value of 1 would prompt the HP to operate at full capacity, and a value in between 0 and 1 would result in a modulated power output. To achieve zonal temperature regulation, the HP input would be determined by the output of the PI controller (Type23) for the mode of operation being selected (dictated by the indoor air temperature as discussed earlier in this section) instead

Table 1
Physical properties and size of different building layers.

Type of envelope	Thermal transmittance	Layers of envelope	Thermal conductivity	Specific capacity	Density	Size
	$W/(m^2K)$	Material	kJ/(h m K)	kJ/(kg K)	kg/m^3	m
Ground floor	0.167	Concrete	1.908	0.84	1280	0.1
		Insulation	0.108	1.21	43	0.169
External wall	0.345	Plaster board	0.576	1.09	800	0.019
		Steel Studs	0.389	1.22	61.77	0.09
		Insulation	0.108	1.21	43	0.05
		Brick	3.204	0.79	1920	0.1
Adjacent wall	0.344	GypBoard	0.576	1.09	800	0.019
		StlStuds	0.389	1.22	61.77	0.09
		Insulation	0.108	1.21	43	0.05
		GypBoard	0.576	1.09	800	0.019
External roof	0.334	Concrete	1.908	0.84	1280	0.1
		Insulation	0.108	1.21	43	0.075
		Roofing	0.504	0.9	530	0.019
Adjacent ceiling	0.488	Concrete	1.908	0.84	1280	0.05
		Insulation	0.108	1.21	43	0.05
		Plaster board	0.576	1.09	800	0.019
External window	1.06	Glass	0.96	0.84	2.5	0.006

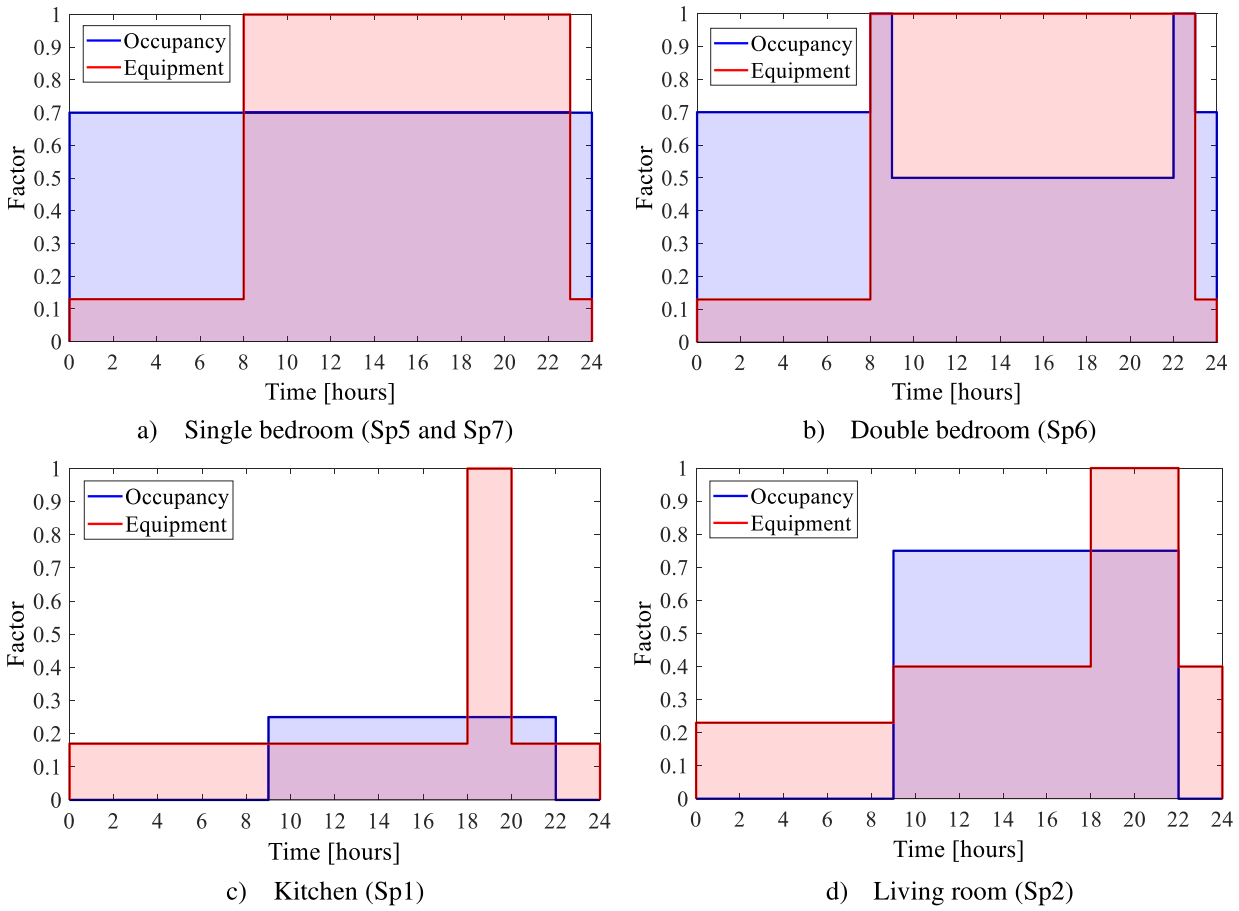

Fig. 5. Daily occupancy pattern of different zones in the investigated residential building.

Table 2
Internal heat gains due to occupancy, equipment, and lighting.

Zone	Number of occupants	Peak load (W)		Occupancy gain (W)	Equipment gain (W)	Lighting gain (W)
		Sensible	Latent			
3-bed: Kitchen (Sp1)	3	225	165	390	300	26.74
3-bed: Living room (Sp2)	3	225	165	390	150	46.64
Bedroom-3 (single, Sp5)	1	75	55	130	80	9.56
Bedroom-1 (double, Sp6)	2	150	110	260	80	21.54
Bedroom-2 (single, Sp7)	1	77	55	130	80	16.98

of using a Type698 thermostat. The PI controller essentially minimises the difference between the measured zone and setpoint temperatures (i.e. the error). It continuously adjusts its output by reacting to the error at the present timestep, while the integral part accounts for past errors. This helps eliminating the steady-state error and improving accuracy in temperature regulation over time.

A HP with a rated heating and cooling capacity of 2 kW (thermal) was selected. The device is responsible for year-round hot water provision, as well as space heating and cooling during different seasons. For the source-side of the HP, a constant water temperature of 10 °C was assumed. This assumption is based on the fact that borehole heat exchangers can provide a stable temperature year-round [48], thus simplifying the model without compromising accuracy.

Two Type158 sensible heat storage tanks were used as buffer tanks to store hot water (i.e. HWTs). In this system configuration, one HWT is used to meet the DHW requirement, while the second one is employed for space heating. The DHW tank (denoted as HWT-1 in Fig. 6) has a storage capacity of 200 Liters, which was selected considering a daily hot water consumption of 100 Liters and the daily hot water draw-off profile shown in Fig. 7. For DHW production, the operation of the HP is regulated through a PI-based control loop to achieve a water supply temperature higher than 65 °C so that the effects of Legionella are eliminated [49]. To ensure this setpoint temperature is achieved, a 500 W auxiliary heater was connected with the DHW tank and regulated by a thermostat (Type106) located at a tank height fraction of 0.9. The role of the auxiliary heater in boosting the water temperature for DHW provision is important as the HP on its own cannot maintain 65 °C during water draw-off. To prevent scalding a tempering valve control was used, which diverts fresh water with the tank supply water in a mixer.

A smaller storage tank (Type158) with a capacity of 100 Liters was exclusively employed to cater for the space heating and space cooling needs (denoted as HWT-2 in Fig. 6). A 139 W auxiliary heater was integrated with the tank to maintain the delivery temperature to 40 °C when there is demand for space heating. The thermostat position and the height fraction of the auxiliary heater input was kept similar to the DHW tank (at a tank height fraction of 0.9). A flow controller was used to manage the load-side flow rate of the HP during both heating and cooling modes. Hot (or cold) water from HWT-2 is pumped to a cross

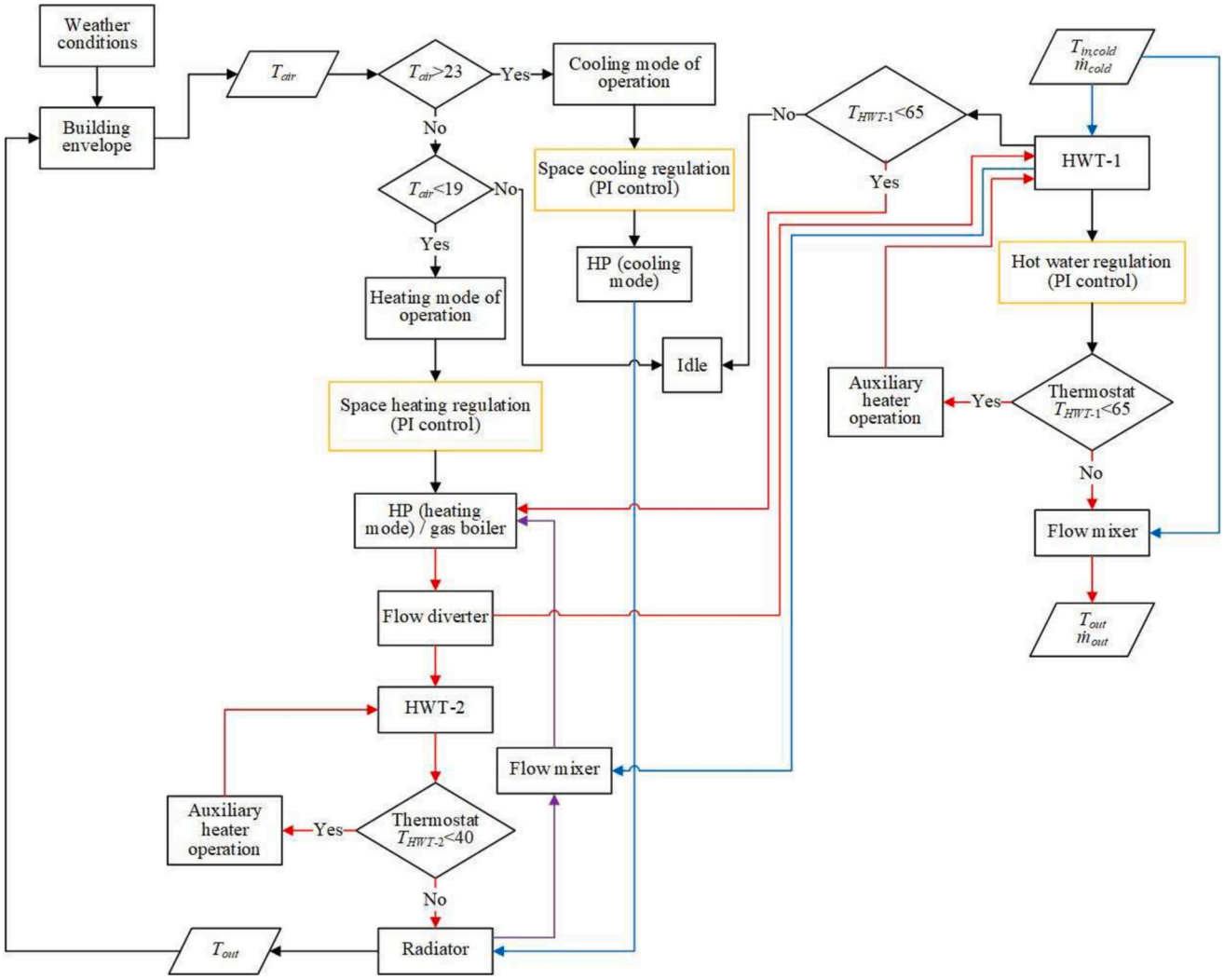

Fig. 6. Flowchart of the energy system operation. The control-related structures (based on PI controllers) are enclosed with a yellow rectangle. The red lines represent the flow of hot water. The blue lines show the flow of cold water. The return flow from the radiator is shown in purple. (For interpretation of the references to colour in this figure legend, the reader is referred to the web version of this article.)

Table 3
Parameters of the PI controllers.

PI controller	HP, space heating operation	HP, space cooling operation	HP, DHW production	Gas boiler, space heating operation	Gas boiler, DHW production
Gain constant	0.1	−0.22	0.1	0.1	0.1
Integral time (hr)	1	0.2	1	1	1

flow heat exchanger (Type140) which heats up (or cools down) the air inside the house. For instance, for space heating operation, the cold air enters the heat exchanger at a flow rate of 10,400 kg/h and the hot air is split between different zones, according to the zone volume, using an air diverting valve (Type646_v2a).

It should be highlighted that in the implemented control strategy demand for space heating was prioritised and met using the heat source (either the gas boiler or the HP). In other words, if there is demand for both DHW and space heating at the same time, the HP's supply is directed to HWT-2. This way, the PI control loop for DHW is not active, the valve to HWT-1 remains closed to ensure the water inside maintains an elevated temperature suitable for domestic use, and the 500 W auxiliary heater is used to entirely meet the DHW demand. The HP supplies HWT-1 only when the tank's water temperature drops below 55 °C, provided there is no simultaneous space heating demand—otherwise, the auxiliary heater ensures an uninterrupted supply of hot water. For a cooling mode of operation, the HP is solely used to deliver space cooling and the auxiliary heater takes full responsibility for hot water provision.

Note: The temperature range for the energy storage system is critical for both safety and operation efficiency. According to established guidelines and the literature, hot water should be stored at a minimum of 60 °C to ensure it reaches at least 50 °C at the outlet of the tank within one minute [50]. This is essential for preventing the growth of Legionella bacteria, which thrive in water temperatures between 20 °C and 45 °C and can cause Legionnaires' disease [49]. Maintaining water temperatures above 50 °C significantly reduces the risk of bacterial growth and ensures the safety of the water supply.

In residential settings, adhering to these temperature standards is crucial for ensuring the health and safety of occupants. The guidelines are based on recommendations from health and safety authorities, such as the World Health Organization and the Centers for Disease Control

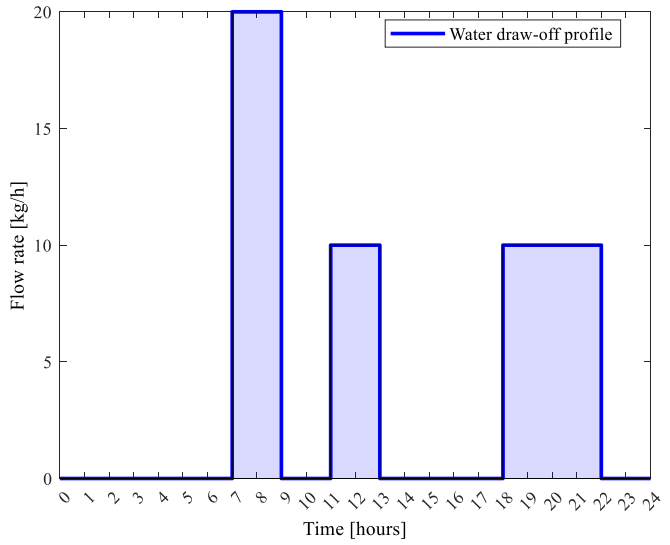

Fig. 7. Daily hot water draw-off profile.

and Prevention, which emphasise the importance of maintaining appropriate water temperatures to mitigate the risk of bacterial contamination [51].

Additionally, maintaining these temperature ranges improves the overall efficiency of the energy storage system. By ensuring that the water is stored and delivered at optimal temperatures, the system can operate more effectively, providing reliable hot water for domestic use while minimising energy consumption. In other words, these standards not only enhance the safety of the water supply but also contribute to the efficient operation of the energy storage system, ensuring both safety and performance in residential buildings.

2.4. Building energy systems

The dynamic energy balance calculations for the house adopted in this paper (see Fig. 3) were also performed using TRNSYS, which solves transient thermodynamic equations. The detailed energy performance analysis requires a complete building model, thermal characteristics of the envelope, definition of heat gains, and occupancy patterns. The simulation time step was set as 0.0083 h, which means the thermodynamic analysis of the entire HVAC system and heat transfer within the building was evaluated at an interval of 0.5 min (30 s). Details of the modelling variables and their values are listed in Table 4. Further information on the mathematical equations and assumptions used for the components employed in the TRNSYS model of the dwelling investigated in this paper can be found in Appendix A.

Two different configurations of the energy system were modelled in this paper. The first configuration simulates the existing energy system where the entire heat demand of the house is met with a gas boiler. In contrast, in the second configuration a reversible HP was utilised to satisfy both heating and cooling demand. Figs. 8 and 9 show both configurations as implemented in TRNSYS. The heating capacities of both the boiler and HP were kept the same to perform a fair comparative analysis. The TRNSYS Type element and design parameters of all key components of the energy system are given in Table 5. The DHW draw-off load profile was modelled using Type14 h. Suitable equations were used in the model to introduce flexibility. For example, the freshwater temperature and flow rate were defined to calculate daily usage of DHW in the equation named “daily load”. Similarly, equations were used in the model to control the flow, operation of the boiler, and to define auxiliary heat inputs.

The storage tanks (HWT-1 and HWT-2) in the systems shown in both Fig. 8 and Fig. 9 were simulated using Type158 of TRNSYS to enhance

Table 4
Details of modelling variables and selected values.

Modelling aspect	Value	Details
House type	Terraced house	Representative of 26 % of UK houses [52].
Construction	Insulated walls	Representative of 60 % of UK houses [53].
Heated floor area	60 m^2	Total floor area of kitchen, living room, and three bedrooms (one double bedroom and two single bedrooms).
Heated zone volume	140 m^3	Total volume of kitchen, living room, and three bedrooms.
Weather data	Energy plus weather (EPW) data file for Cardiff, Wales, UK	Historical weather data for year 2022 [39].
Heating and cooling setpoint temperature	19 °C and 23 °C	Following the CIBSE Guide A [43].
Boundary temperature	Identical	The adjacent houses on both sides are assumed to be at the same temperature.
Ground temperature	10 °C	A simplified model for heat loss through ground is used, wherein heat transfer is determined by assuming a ground temperature that matches the average annual air temperature [43].
Infiltration rate	0.4 air change per hour (ACH)	Following standard TM59 from CIBSE [42].
Internal heat gains due to lighting, occupancy, and equipment	The hourly heat gain due to occupancy, equipment, and lighting is calculated by multiplying the total heat gain (Table 2) with the usage profiles (Fig. 5). A constant lighting gain of 2 W/m^2 is used for all zones (multiplied with the floor area of each zone to calculate heat gain). Lights are turned on between 18:00 to 23:00 h only.	Following standard TM59 from CIBSE [42]. A thermal capacitance of ten times the air capacitance in each zone was assumed to compensate for curtains, furniture, and other material objects in the residential building (see Appendix B).

the performance of the HP system by minimising frequent cycling—thus improving efficiency and extending lifespan [54]. The use of separate tanks for DHW and space heating allows a better control, as DHW requires higher temperatures than space heating. This configuration enables stable operation for the HP and prevents frequent temperature adjustments, improving overall efficiency [55].

Having two tanks—or a partitioned single tank—helps manage different thermal demands efficiently using thermal stratification. The larger storage capacity also allows for longer, more efficient HP operation cycles, minimising energy losses [56]. Operationally, separate tanks make maintenance simpler and reduce system downtime, further improving reliability. Overall, this approach improves system flexibility, enhances HP efficiency, and helps manage seasonal and operational demands effectively, contributing to better performance and energy savings [54].

3. Verification of the multi-zone modelling approach

To ensure the reliability of the multi-zone building model implemented in TRNSYS, a verification exercise was carried out using data from an experimental study found in the literature [57]. The experiment involved continuous monitoring of indoor and outdoor temperatures in a real semi-detached house located in Loughborough, UK. The front view and rear view of the dwelling are shown in Fig. 10. For

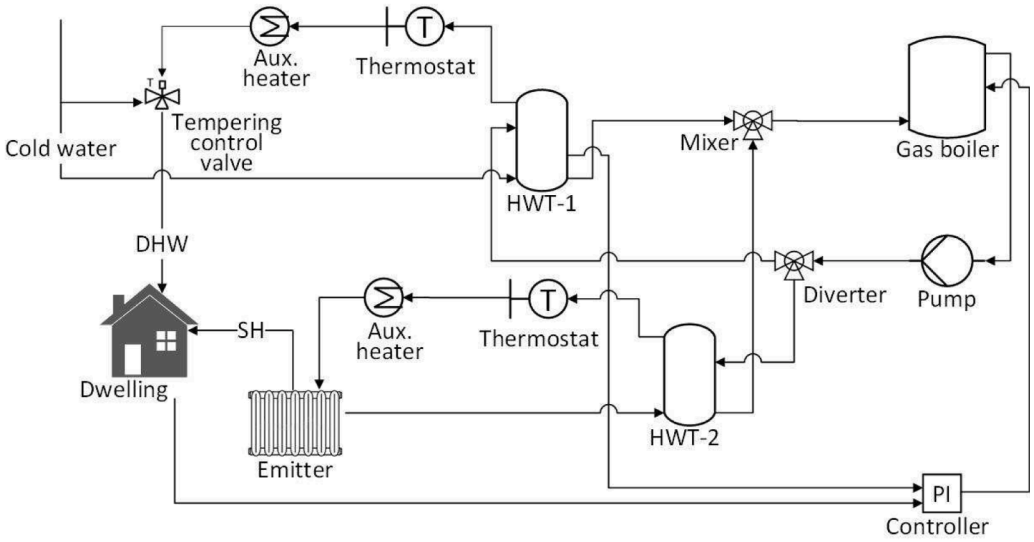

(a)

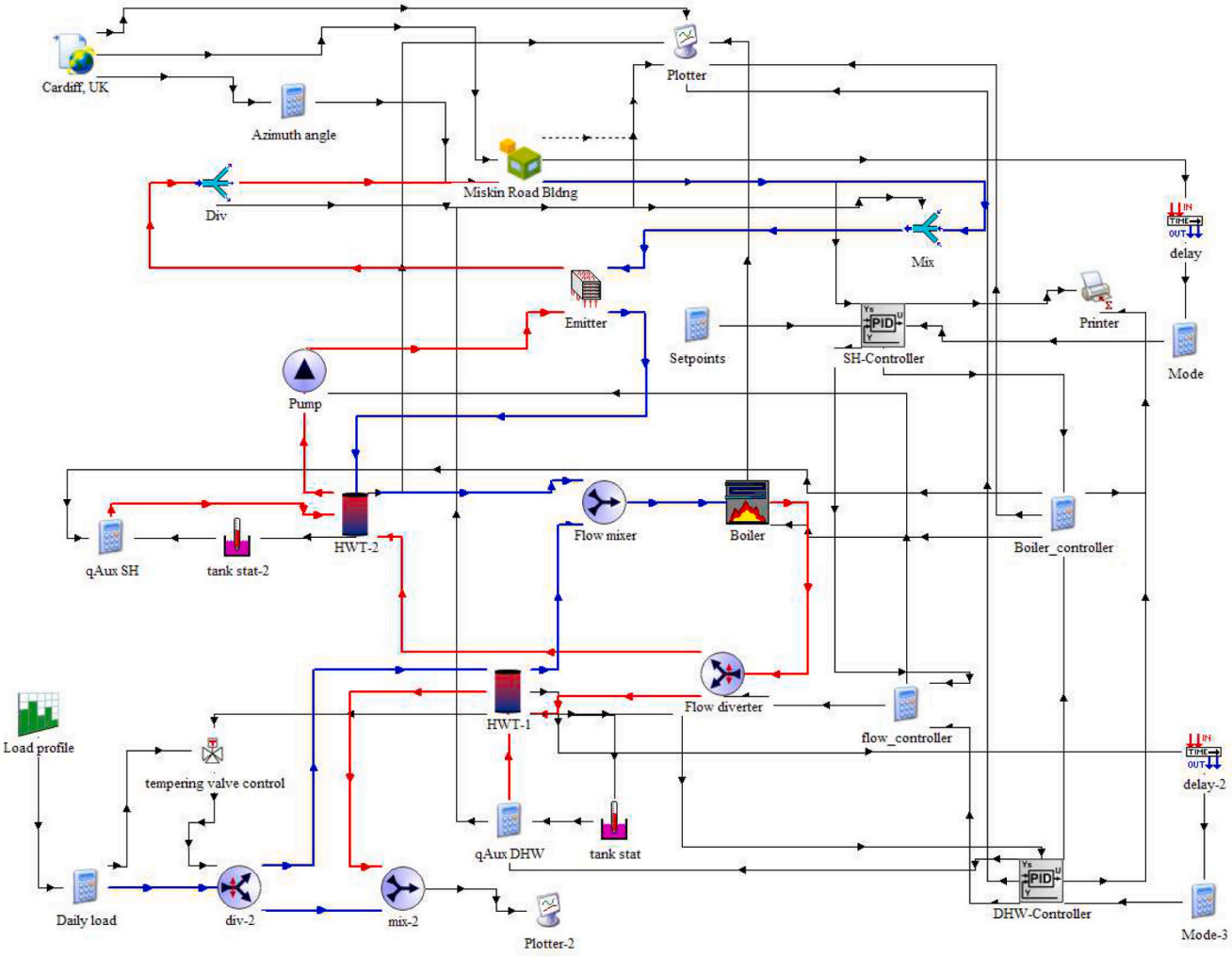

(b)

Fig. 8. Energy system with a boiler to meet heat demand. (a) Block diagram. (b) Schematic in TRNSYS.

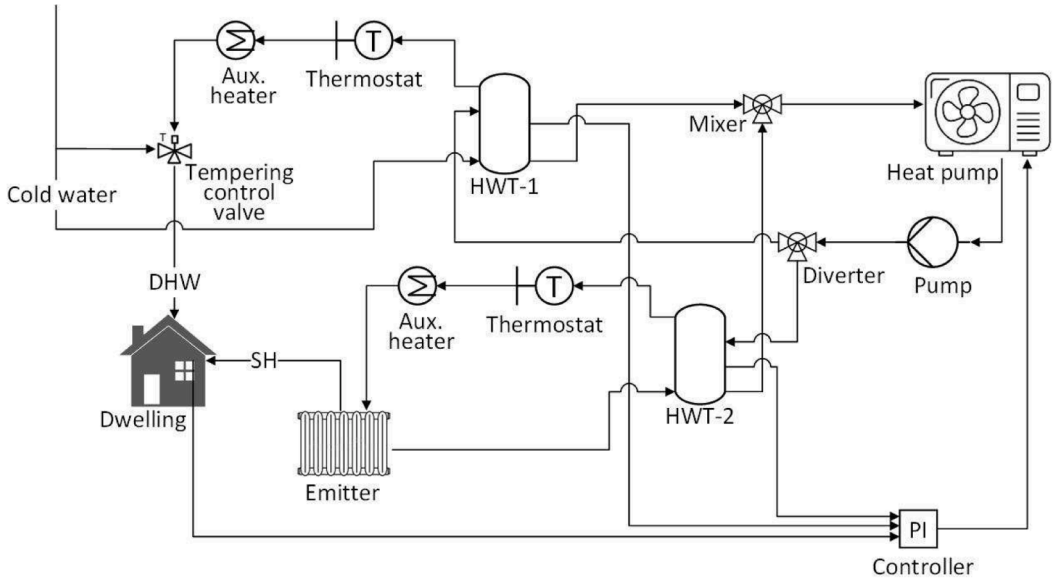

(a)

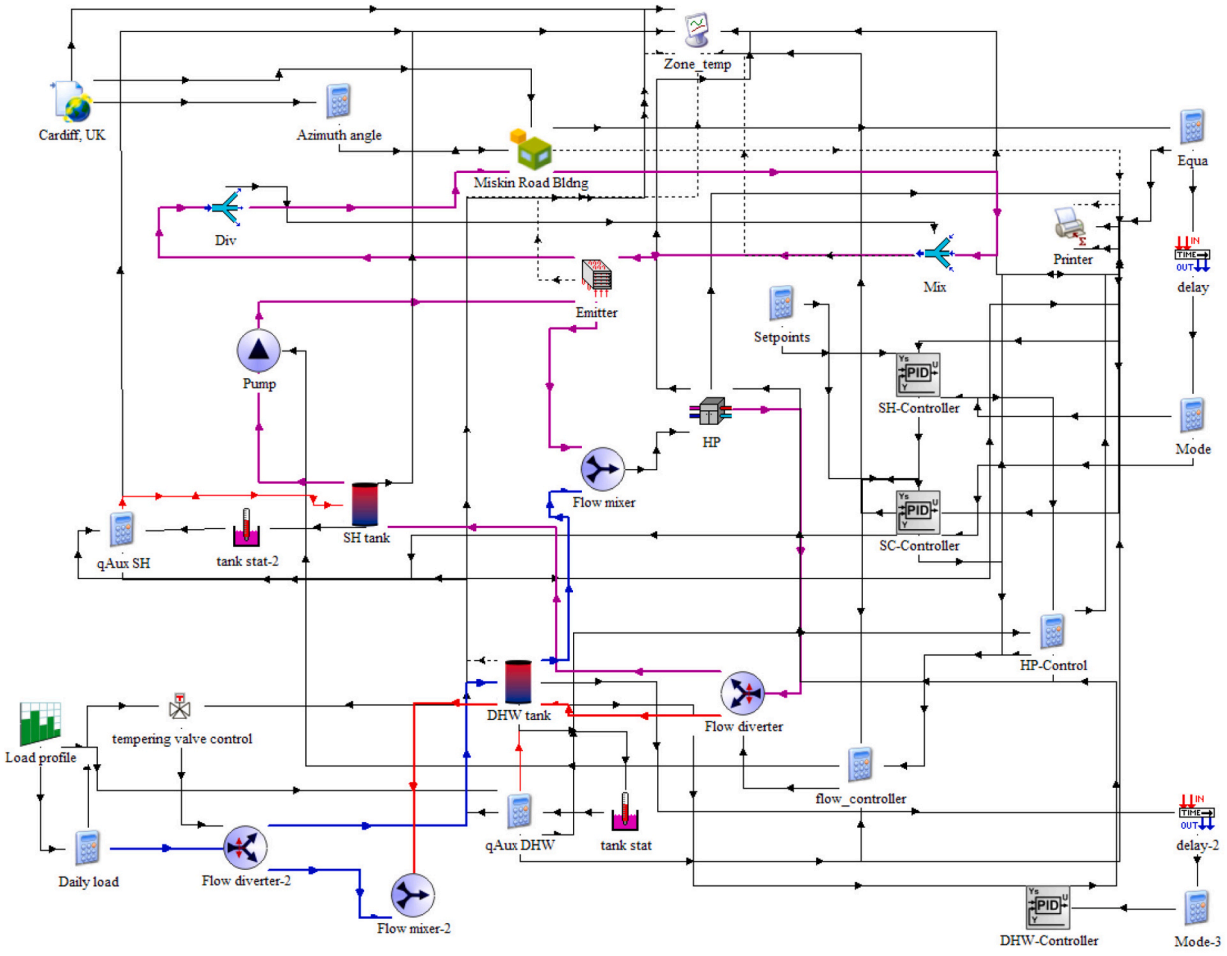

(b)

Fig. 9. Energy system with a HP to meet heat and cooling demand. (a) Block diagram. (b) Schematic in TRNSYS.

Table 5
TRNSYS type and design parameters of energy system components.

Component	Type	Parameters	Value	Units
Weather conditions	15–3	Library/Location	Energy+ Weather Files (EPW)	
Building model	56			
Boiler	700_v2a	Rated capacity	2	kW
		Fluid specific heat	4.19	kJ/(kgK)
		Setpoint temperature	85	C
		Boiler efficiency	0.9	–
		Combustion efficiency	0.9	–
HP	9271	Source/load fluid specific heat	4.19	kJ/(kgK)
		Source/load fluid density	1000	kg/m^3
		Rated cooling capacity	2	kW
		Rated cooling power	0.4	kW
		Rated heating capacity	2	kW
		Rated heating power	0.4	kW
		Rated source/load flow rate	0.4	l/s
		Inlet source temperature	15.56	C
		Inlet load temperature	37.78	C
Storage tank	158	DHW tank volume	200	l
		SH tank volume	100	l
		Tank height	1.11	m
		Number of tank nodes	5	–
		Fluid specific heat	4.182	kJ/(kgK)
		Fluid density	992	kg/m^3
		Fluid thermal conductivity	2.224	W/(mK)
		Height fraction of inlet 1	0.65	–
		Height fraction of outlet 1	0	–
		Height fraction of inlet 2	0	–
		Height fraction of outlet 2	1	–
		Height fraction of thermostat	0.9	–
		Height fraction of auxiliary input	0.9	–
Heat exchanger	140	Inlet fluid temperature	40	C
		Inlet fluid flow rate	300	kg/h
		Inlet air temperature	10	C
		Inlet humidity ratio	0.003	–
		Inlet air flow rate	10,400	kg/h
		Total heating capacity	10	kW
Air diverting valve	646_v2a			
Flow mixer	11 h			
Flow diverter	11f			
Load profile	14 h			
Tank thermostat	106			
PI controller	23	Gain constant/integral time	See Table 3	

completeness, the verification also involved a comparison against results obtained using other software packages commonly employed for building simulation. To this end, the same dwelling shown in Fig. 10 was modelled and simulated in IES VE and Modelica using the approach documented in [58–60].

The construction materials and dimensions of the house were sourced from [57] to develop an equivalent model in TRNSYS. The screenshot of the model developed in SketchUp is shown in Fig. 11. Some geometric simplifications were made: bay windows were represented as standard windows, chimney ducts were excluded, and the front entrance door was simplified. The building's thermal envelope was simulated as described in Section 2. A multi-zone modelling approach in TRNSYS Type56 was used, with the heating system omitted, as it was not assessed in the experiment conducted in [57]. An air infiltration rate of 0.22 air change per hour (ACH) was adopted based on the experimental setup. The hourly outdoor temperatures recorded between June and September 2021 were used as the ambient boundary condition. Solar radiation effects were incorporated using the internal radiation calculation method, taking into account the house's orientation.

During the experiment, the indoor temperature was monitored hourly in each room of the house and the TRNSYS model was simulated for the same period. Results are shown in Fig. 12 for selected rooms (kitchen, rear double bedroom, dining room, and living room). The figure also includes experimental data available in [57]. The simulated indoor temperatures (red trace) exhibit a reasonably good agreement

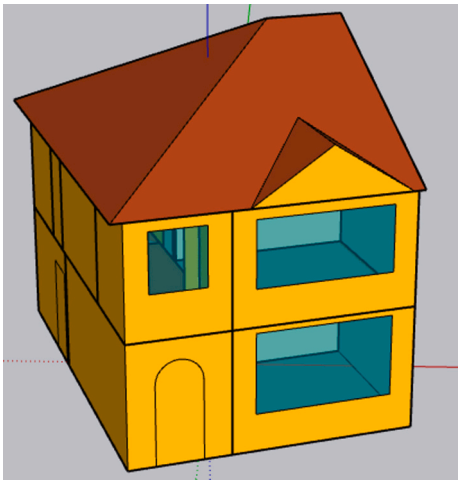

Fig. 11. Screenshot of building model 'west house' developed in SketchUp.

(a) (b)

Fig. 10. The matched-pair houses used in the experiments [57]: (a) Front view (b) Rear view. The west house shown on the left in (a) was modelled for verification.

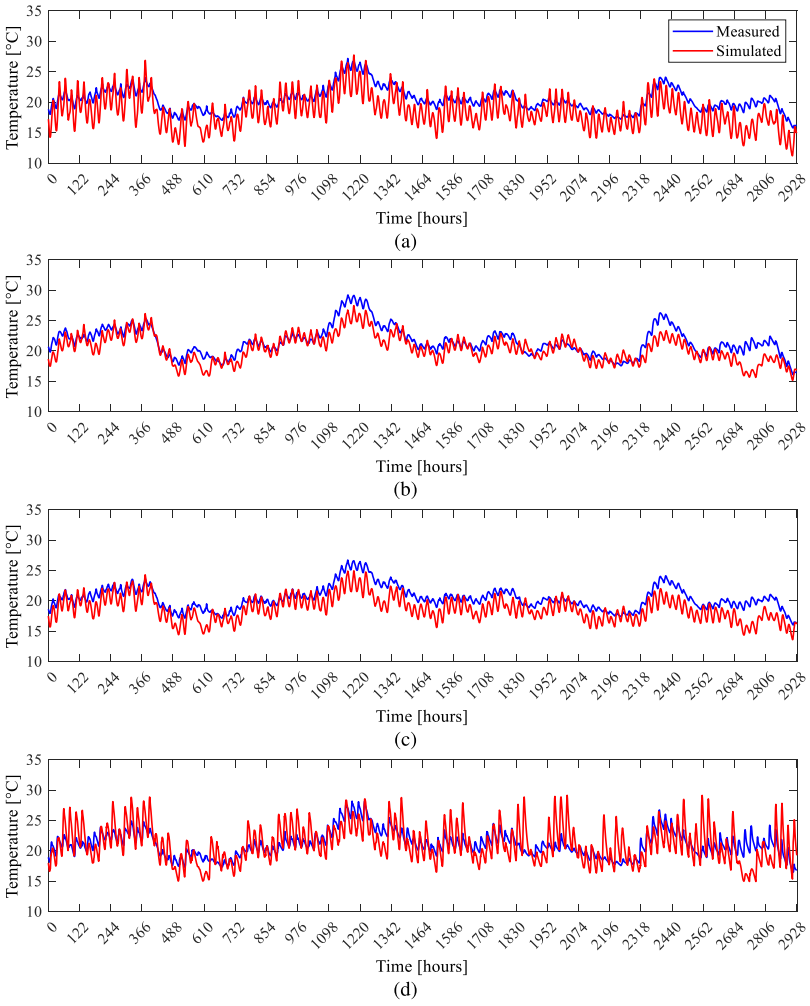

Fig. 12. Verification of the house model implemented in TRNSYS with experimental measurements in [57]: (a) Kitchen. (b) Rear double bedroom. (c) Dining room. (d) Living room.

with the experimental data (blue trace), although some differences can be noticed. These discrepancies can likely be attributed to the approximation of measured solar radiation with TRNSYS-computed values, which may have led to differences in heat transfer rates from the external environment to the building. This, in turn, affected the indoor temperature predictions.

To quantitatively assess the validity of the simulation results, the mean absolute error (MAE) and the root mean squared error (RMSE) between the set of experimental data and simulated temperatures were calculated for each room. The metrics for all rooms in the house are provided in Table 6. These metrics, alongside the visual representation in Fig. 12 demonstrate that a reasonable level of accuracy is achieved despite the data availability limitations and simplifications in the building model.

To further verify the effectiveness of the modelling approach, an additional comparison was conducted against simulation results obtained using another software package. The same dwelling shown in Fig. 10 was simulated in IES VE as discussed in [59] and results were monitored hourly in each room of the house. Fig. 13 shows the indoor temperature for selected rooms. The blue trace shows the experimental data available in [57], while a red trace shows the results obtained with TRNSYS and the green trace the results using IES VE. The error metrics are also presented in Table 6. As observed, both software engines lead to relatively similar indoor temperature performance. These results further enhance the credibility of adopting TRNSYS in this paper.

When looking more closely at Table 6, the simulation results obtained using IES VS exhibit a higher accuracy compared to those obtained with TRNSYS. This can be explained by the simplifications made for the building model in TRNSYS. While the bay windows were modelled in IES VE, these were not incorporated in TRNSYS. More

Table 6
MAE and RMSE between the experimental data and simulation results.

Room	Software Engine	MAE (°C)	RMSE (°C)
Kitchen	IES VE	1.64	1.88
	TRNSYS	2.13	2.47
Front double bedroom	IES VE	1.17	1.45
	TRNSYS	1.80	2.32
Hall	IES VE	1.68	1.93
	TRNSYS	2.26	2.61
Rear double bedroom	IES VE	1.44	1.80
	TRNSYS	1.35	1.69
Dining room	IES VE	1.40	1.60
	TRNSYS	1.76	2.02
Living room	IES VE	1.39	1.67
	TRNSYS	1.81	2.34
Single bedroom	IES VE	1.08	1.36
	TRNSYS	1.99	2.45
Landing	IES VE	1.56	2.10
	TRNSYS	1.98	2.32
Loft	IES VE	2.86	3.35
	TRNSYS	3.27	4.56
Bathroom	IES VE	1.66	2.11
	TRNSYS	2.02	2.37

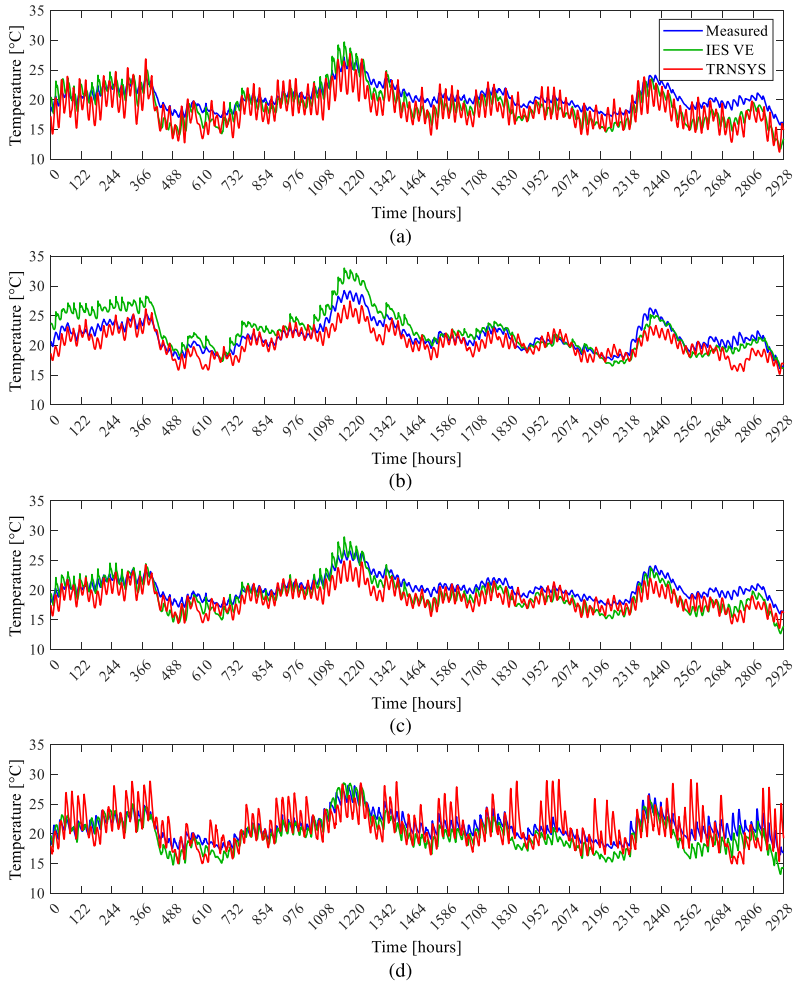

Fig. 13. Verification of the house model implemented in TRNSYS and IES VE with experimental measurements in [57]: (a) Kitchen. (b) Rear double bedroom. (c) Dining room. (d) Living room.

importantly, only the west house was modelled in TRNSYS using an adjacent wall boundary condition with no solar gains, whereas both the east and west houses were modelled in IES VE.

A final verification exercise was conducted. In this case, the dwelling was simulated but following the approach adopted in [60]. In the reference, simulations were conducted using Modelica but the house model was assumed to consist of the entire indoor volume as a whole without considering any room partitioning. The measured values in the experiment presented in [57] were weighted based on the individual room volume and averaged. For consistency, the simulation was conducted between June and September 2021. Fig. 14 shows a comparison of the results obtained with TRNSYS (red trace), Modelica (green trace, as presented in [60]) and experimental data (blue trace, with averaged results reproduced from [60]). For completeness, results obtained with

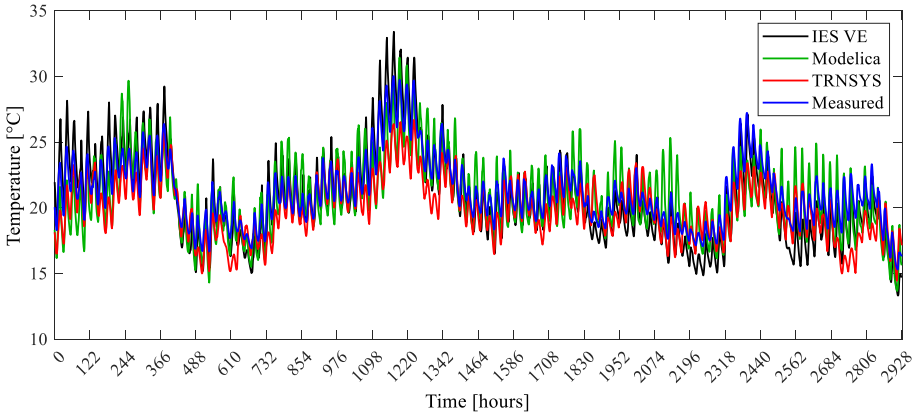

Fig. 14. Verification of the house model implemented in, IES VE (black trace), Modelica (green trace) and TRNSYS (red trace) with experimental measurements in [57] (blue trace). Averaged indoor temperature. (For interpretation of the references to colour in this figure legend, the reader is referred to the web version of this article.)

IES VE are also shown (black trace). This trace for IES VE represents the average indoor temperature after the different individual room temperatures have been weighted. Table 7 compares the RMSE between simulation results and the experimental data, with the three software engines providing a reasonable level of agreement. Although there are minor discrepancies in the error metrics, these are deemed acceptable considering the differences in the modelling approaches adopted for each software.

The results presented in this section alongside the comparison against experimental data and results using other software packages provide confidence in the multi-zone modelling approach adopted in this paper and the suitability of TRNSYS.

4. Results and discussion

4.1. Meeting heat demand with a boiler

The energy system configuration where a gas boiler is responsible for space heating and DHW provision of the house was investigated first. A boiler with an efficiency of 90 % was used. Fig. 8 shows a block diagram of the energy system and a schematic of its TRNSYS implementation. A simulation incorporating a detailed three-dimensional model of the house, occupancy, lighting, equipment utility patterns, and internal heat gains was performed for an entire year using the historical weather data of Cardiff for year 2022 shown in Fig. 2. The temperature variation shows a high temperature in the middle of the year while low temperatures are seen in the beginning and end of the year. Based on the year round temperature profile, detailed results are shown only for January and August to representatively account for the winter and summer seasons.

Fig. 15 shows the outdoor temperature profile during the cold winter and hot summer days under investigation. Fig. 16 shows the temperature profile inside different rooms of the house when a gas boiler is used for space heating and hot water provision. During winter (see Fig. 16a), the boiler circulates hot water through the radiator when the indoor temperature drops below the heating setpoint of 19 °C, thereby increasing the room temperature. The PI controller effectively maintains the indoor temperature of the different zones above the setpoint. Minor temperature fluctuations between 04:00 and 11:00 arise whenever the kitchen temperature briefly falls below the setpoint, prompting the controller to react (this reflects in turn in small variations in the energy supplied by the boiler, not shown). The observed temperature variations between rooms reflect the thermal interactions between the building envelope and the outdoor environment. Furthermore, the temperature discrepancies among rooms highlight the influence of factors such as room orientation, internal heat gains, and local thermal mass effects on temperature regulation.

During summer when there is no space cooling device (see Fig. 16b), the indoor temperature mirrors the outdoor temperature profile (this is shown in Fig. 15b). This trend underscores the building's susceptibility to overheat during warmer periods. Such conditions emphasise the importance of integrating adaptive systems, like reversible HPs, capable of addressing both heating and cooling needs. Implementing such systems can mitigate temperature fluctuations in winter and alleviate overheating risks in summer, ultimately enhancing energy efficiency and maintaining indoor thermal comfort throughout the year.

Fig. 17 shows the hourly energy consumption of the boiler on the left axis and the energy input to HWT-1 by the auxiliary heater on the right axis during a typical hot day and a typical cold day in 2022 (13th August and 15th January). As shown in Fig. 17a, during the winter day, the boiler operates throughout the day to maintain indoor thermal comfort and provide hot water for domestic use. During the summer day, as shown in Fig. 17b, the boiler's usage is slightly reduced as it only functions to meet the DHW requirements.

The highest energy consumption by the boiler on the cold day occurred in the morning (1.92 kWh at 09:00), which corresponds to a simultaneous increase in space heating and DHW demand. The auxiliary heater also contributes during these hours to meet this increased energy demand. This surge can be linked to occupancy-related activities, such as morning showers and increased heating needs following the overnight temperature setback. Through the rest of the day, the auxiliary heater did not contribute to maintaining the DHW temperature at 65 °C, highlighting the boiler's capability to meet space heating and DHW demands independently.

As shown in Fig. 17b, the boiler's energy consumption during the summer day followed a similar pattern as during winter. This is because the DHW demand was assumed uniform for each day throughout the year with a peak of 1.53 kWh at 10:00, coinciding with a scheduled hot water draw-off from 11:00 (see Fig. 7). The reduced energy consumption of the boiler is due to the absence of any space heating needs during the summer warmer day. The auxiliary heater was not operational during this period, as the DHW requirements were met by the boiler alone. Over the entire year, the auxiliary heater provided an average energy supply of only 5.73 kWh to HWT-1 in January (not shown), further reinforcing the boiler's adequacy in meeting space heating and DHW production demands without significant supplementary heating.

The average monthly energy consumption of the boiler configuration for year 2022 is shown in Fig. 18. The highest consumption values occurred during the colder winter months, with a peak of approximately 349.33 kWh in January, followed by 343.26 kWh in December. This trend reflects the substantial space heating requirement during periods of low ambient temperatures, when heat losses to the external environment are most pronounced due to the large temperature differential between indoor and outdoor conditions.

As expected, energy demand drops significantly after January, as the boiler is predominantly used to meet DHW needs rather than space heating demand. The lowest monthly energy consumption, 243.75 kWh, occurred in February. Beyond this, the energy demand had a relatively uniform level throughout the rest of the year.

During the summer months, when the boiler is used exclusively for DHW provision, energy consumption remains relatively steady at lower levels. This suggests that the gas boiler is slightly oversized during these periods, operating inefficiently at partial load conditions. The year-round variability in consumption points towards the need for a more adaptable heating system, such as a reversible HP, which can modulate its operation based on seasonal demand. Implementing such a system could potentially enhance overall energy efficiency and reduce operating costs, especially during periods of low demand. This is explored in Section 4.2.

Note: The reduced energy consumption of the gas boiler during the colder months of February and March is a direct consequence of the reduced space heating demand due to internal heat gains. These gains are due to occupancy, lighting, and appliances and, in this case, contribute to indoor temperature and compensate the space heating demand of the house. The influence of internal heat gains on energy consumption is analysed in more detail in Section 4.3.

Table 7
RMSE between the experimental data and simulation results using different software engines.

Software engine	MAE (°C)	RMSE (°C)
TRNSYS	1.48	1.85
IES VE	1.15	1.40
Modelica	1.25	1.56

4.2. Meeting heating and cooling demand with a HP

Fig. 19 shows the indoor temperature variations for the energy system using a reversible HP during a cold day (15th January, Fig. 19a) and a hot day (13th August, Fig. 19b). The outdoor temperature profile is given in Fig. 15 for both days. During the cold day, the HP system

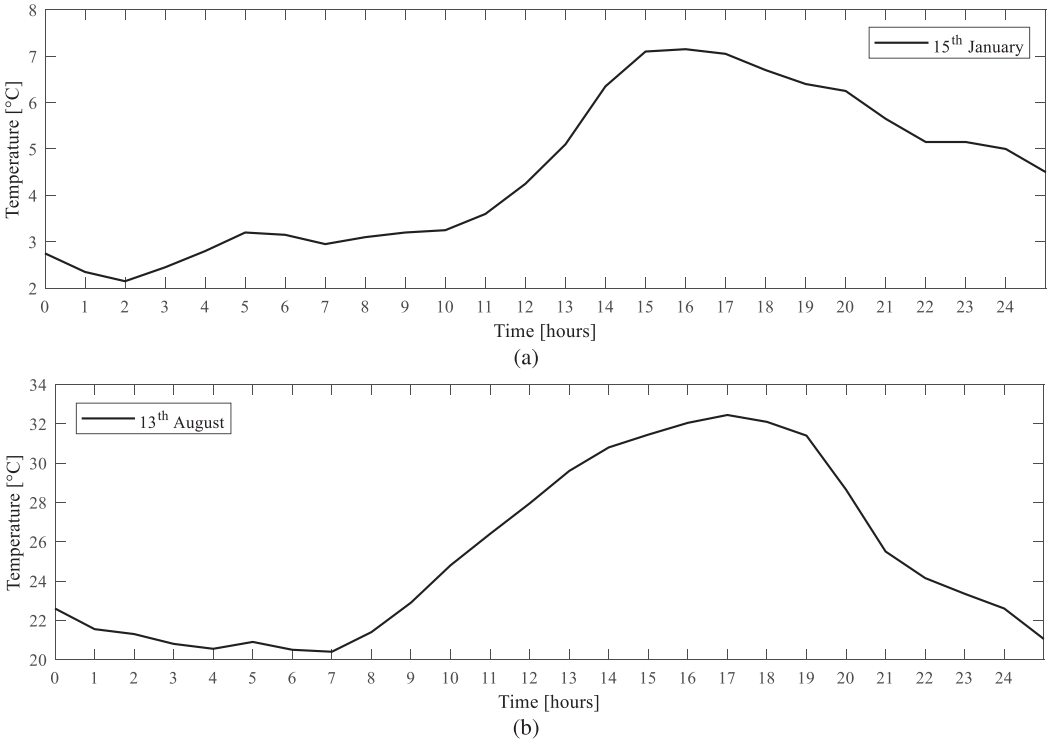

Fig. 15. Outdoor temperature on a) 15th January and b) 13th August.

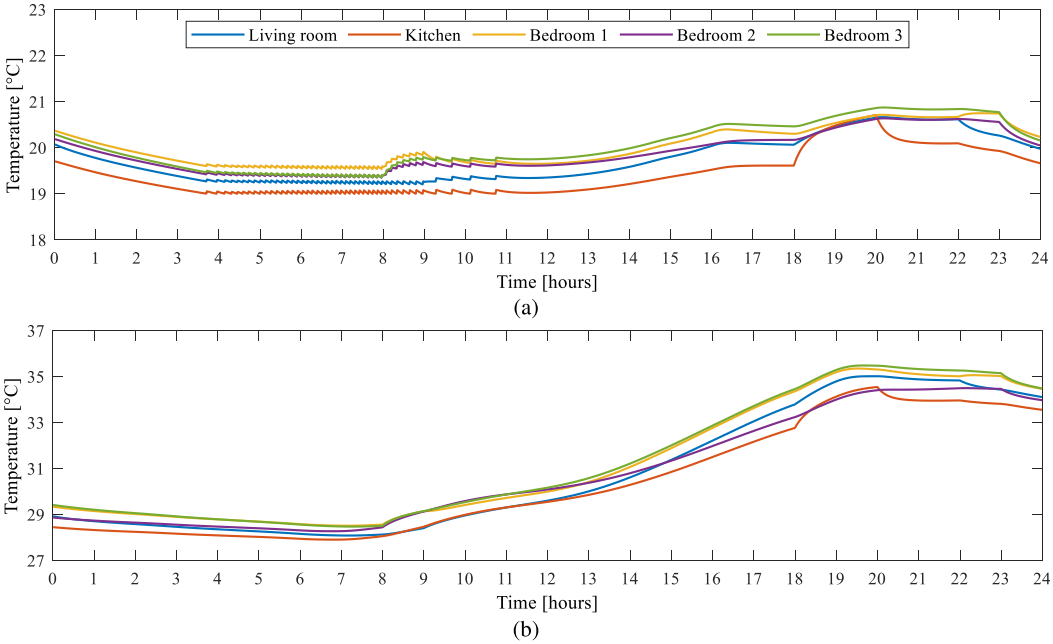

Fig. 16. Temperature control in different zones through boiler on a) 15th January and b) 13th August.

effectively maintains temperatures across the thermal zones, similar to the boiler-based system discussed in Section 4.1 (see Fig. 16a). This is achieved by the PI control-based scheme, which ensures the HP is operated to maintain the temperature close to the heating setpoint of 19 °C. The stratification in different room temperatures can be attributed to the flow distribution and the thermal load in each zone.

In contrast, during the hot day (Fig. 19b), the room temperatures are maintained around the cooling setpoint of 23 °C. A notable temperature rise in the kitchen space (Sp1) takes place at 18:00 followed by a drop at 20:00. This is consistent with internal heat gains due to electrical appliances usage. Similar temperature variations are observed at different time intervals such as 08:00, 22:00, and 23:00 for other thermal zones, which coincides with the occupancy and equipment internal heat gain pattern shown in Fig. 5 (see Section 2.2).

Fig. 19 highlights the influence of the HP during typical summer and winter days. To analyse its performance in more depth, the heating and cooling loads met by the HP on the representative cold winter day and hot summer day are shown in Fig. 20. For clarity, the figure includes the

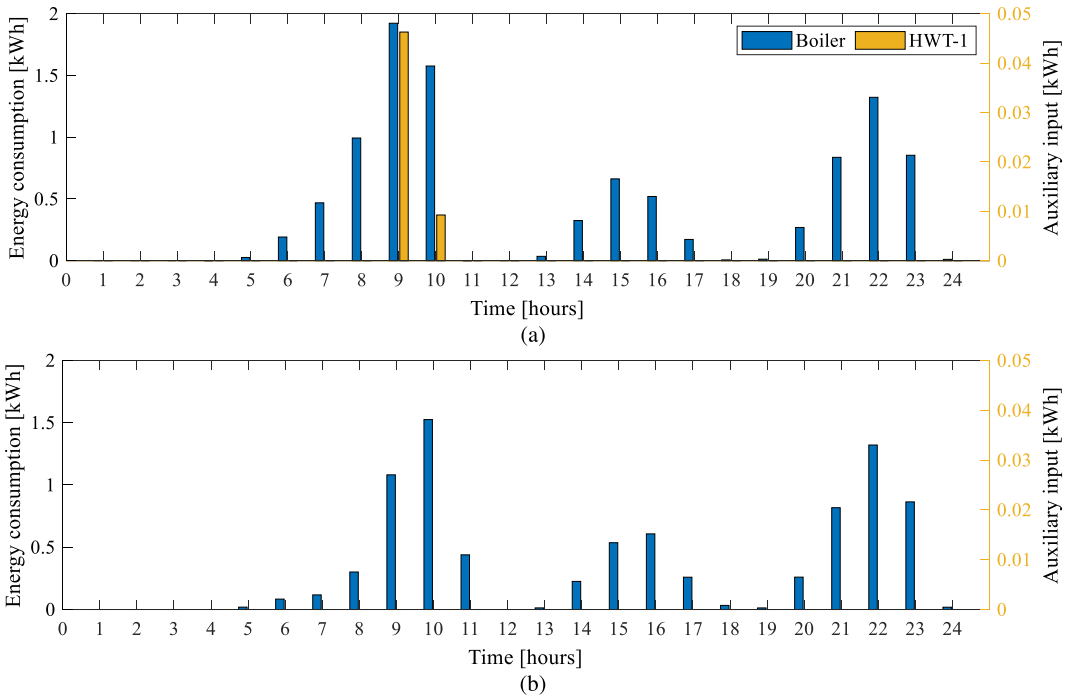

Fig. 17. Energy consumed by boiler on a) 15th January and b) 13th August.

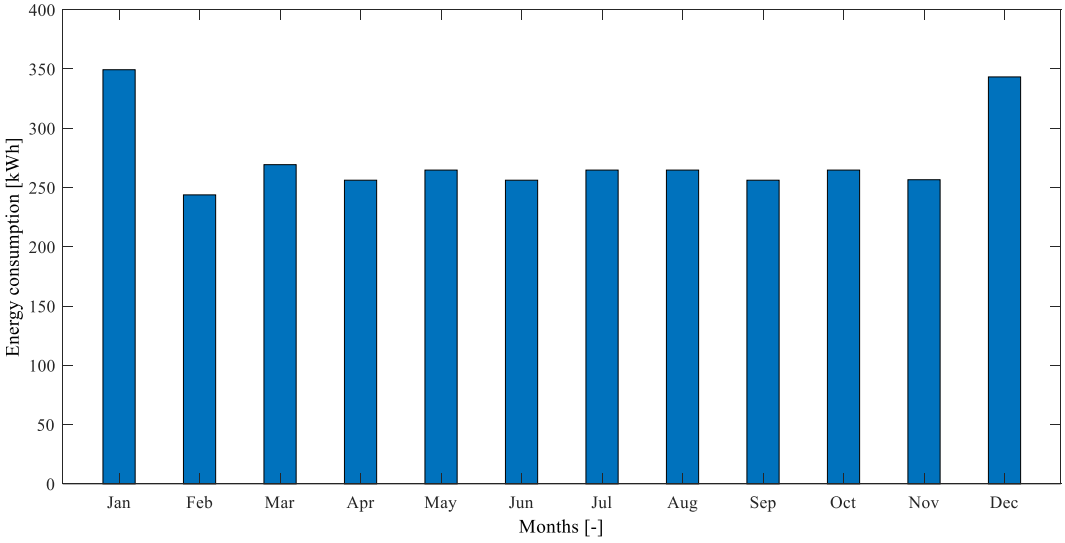

Fig. 18. Monthly energy consumption by boiler configuration.

ambient temperature, shown with a yellow trace, providing crucial context to understand the HP behaviour under different thermal demands.

Focusing on the cold day scenario (Fig. 20a), the HP meets the heat demand during the early morning hours when the ambient temperature drops to its lowest levels. The morning space heating loads occur from 05:00 till 08:00, but a notable peak in thermal load is observed at 09:00, reaching 1.95 kWh, coinciding with the morning DHW requirement. This simultaneous demand highlights the dual functionality of the HP in providing space heating and DHW. The maximum heating load of the day occurs at 22:00, reaching 2.18 kWh. This peak corresponds to the evening DHW requirement and decreasing outdoor temperature, in turn indicating an increased space heating demand, and the HP effectively responds by ramping up its output. Throughout the day, the HP adjusts its output to respond to varying thermal demands, showcasing its capability to maintain indoor thermal comfort despite fluctuating ambient conditions.

In contrast, on the hot summer day (Fig. 20b), the HP operates only in cooling mode to counteract the elevated indoor temperatures that exceed the cooling setpoint for most of the day. During the early morning hours (before 08:00), minimal cooling contributions from the HP are required as the outdoor temperature remains below 24 °C. However, as the day progresses, the cooling demand increases substantially in response to rising outdoor temperature, reaching 32.5 °C around 17:00. The HP responds to the increased demand, reaching its maximum cooling load of 2.32 kWh at 20:00, and operating slightly above its rated (thermal) capacity for a few hours. The sustained operation of the HP during such a usually hot day underscores its role in mitigating thermal discomfort under extreme weather conditions.

The electrical energy consumed by the HP is shown in Fig. 21. On the

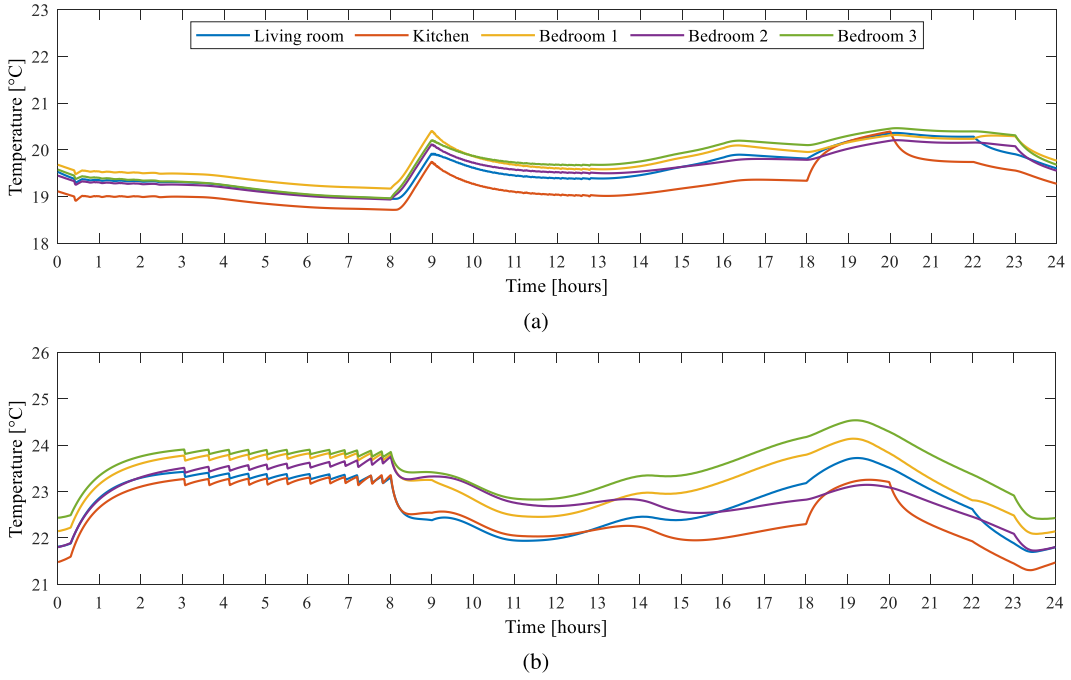

Fig. 19. Temperature control in different zones through HP on a) 15th January and b) 13th August.

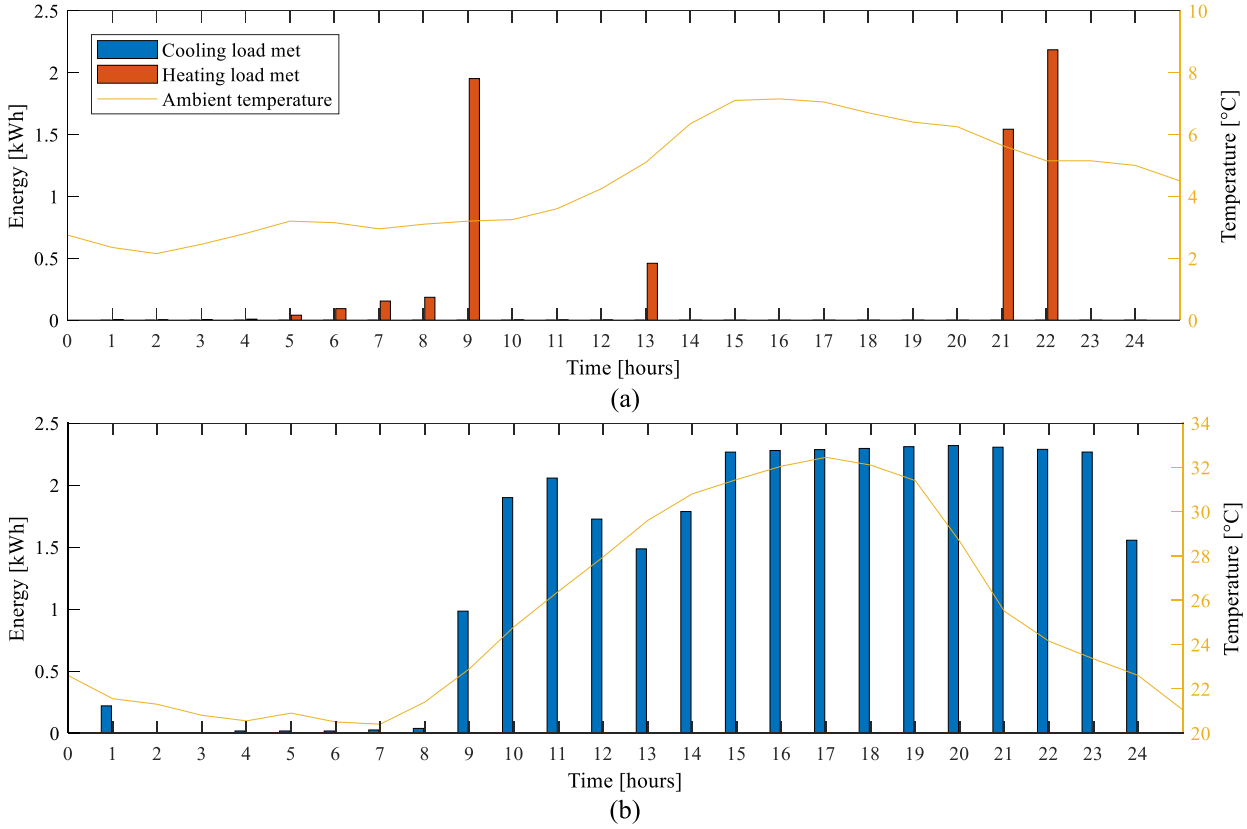

Fig. 20. Energy load met by HP on a) 15th January and b) 13th August.

cold winter day (Fig. 21a), the HP's energy consumption closely follows the heating demand, with a notable peak of 0.35 kWh at 22:00. This corresponds with the highest heating load of the day, reflecting the HP's increased operational demand to maintain indoor thermal comfort during the coldest hours. The consumption pattern demonstrates the HP's efficiency in modulating power based on thermal demand, providing minimal energy input during periods of lower heating requirements, such as the early morning, and ramping up power when the heating demand is substantial. This adaptive behaviour underlines the energy system's capability to respond to dynamic thermal loads while

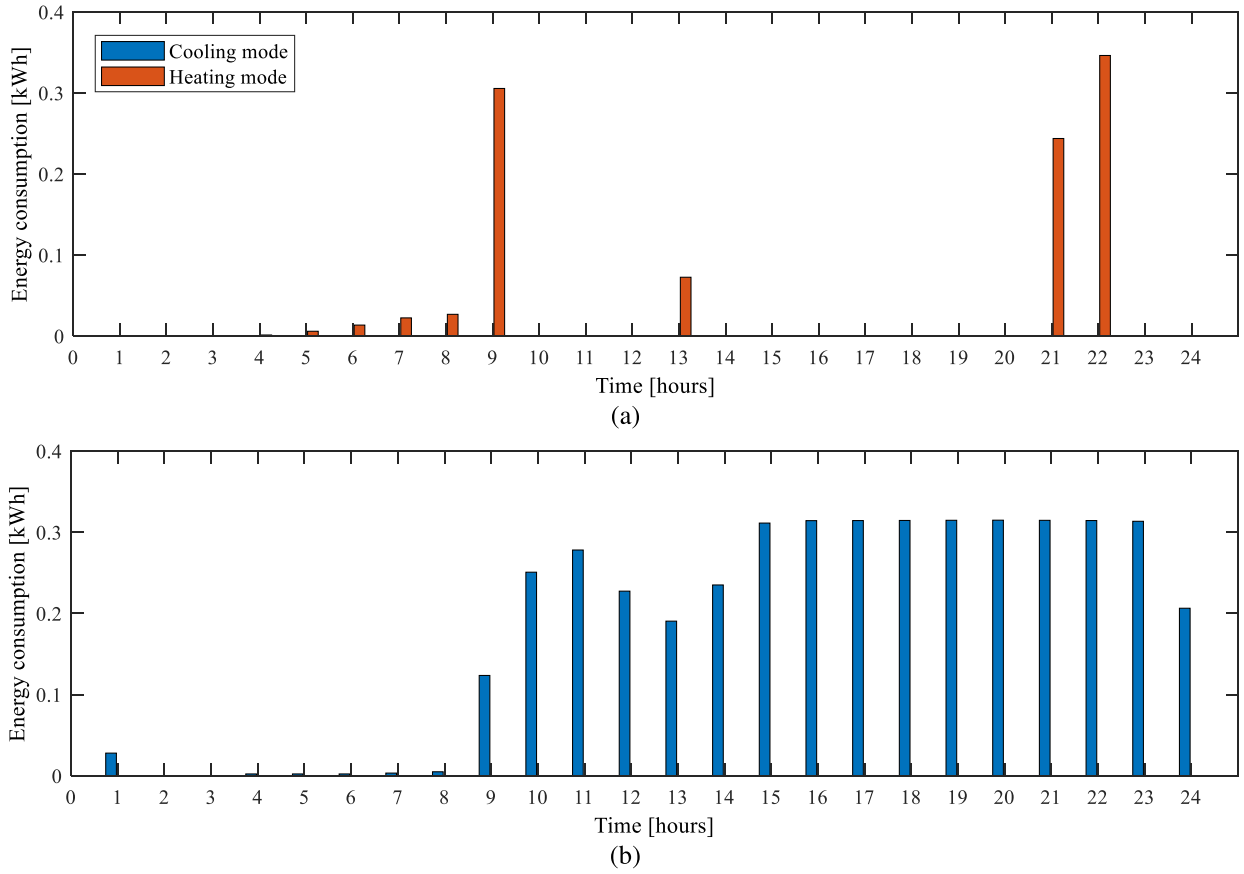

Fig. 21. Energy consumed by HP on a) 15th January and b) 13th August.

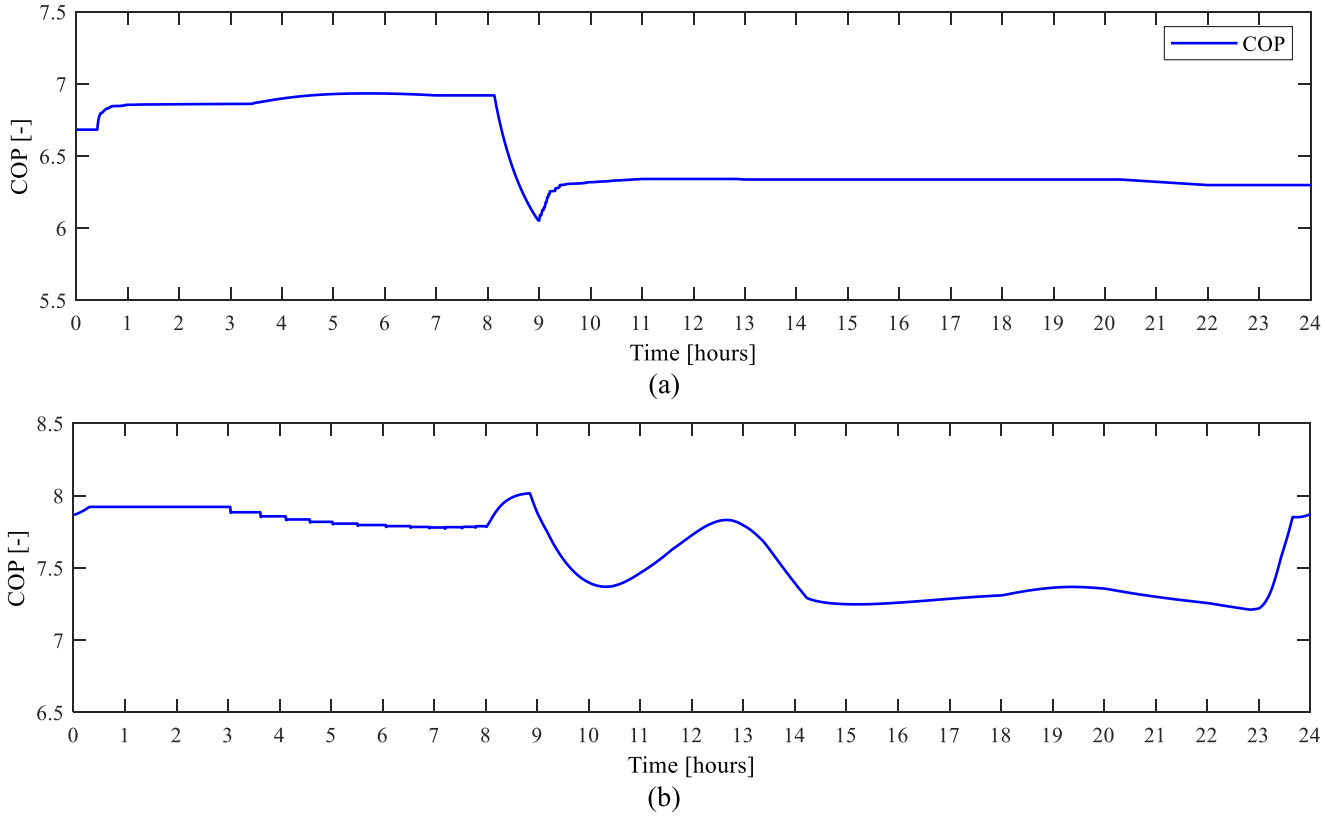

Fig. 22. COP of HP on a) 15th January and b) 13th August.

optimising energy usage.

Conversely, on the hot day (Fig. 21b), the HP operates only in cooling mode, with energy consumption peaking at 0.315 kWh at 20:00. This peak coincides with a prolonged period of elevated cooling demand, driven by high outdoor temperatures exceeding 32 °C. Unlike the winter scenario, the HP operates consistently throughout the day to maintain thermal comfort in the house. The energy consumption in cooling mode is thus higher compared to the heating mode, reflecting higher space cooling demand during these particular weather conditions. As for the DHW demand, this is instead met by the auxiliary electric heater, as the HP prioritises space cooling (as described in Section 2.3). This finding highlights the importance of integrating a responsive auxiliary heating system to manage DHW demand during periods when the HP is otherwise engaged.

The HP operation during the cold and hot days underscores the device's adaptability to different requirements and its capability to meet thermal demand efficiently. The differences in energy consumption reflect the varying nature of thermal needs as a result of weather conditions, with the HP exhibiting a robust performance under both heating and cooling modes.

Fig. 22 illustrates the HP's COP across a 24-h period on the winter and summer days. The COP, which is a measure of energy efficiency, reflects the ratio of the useful thermal energy delivered by the HP (for heating or cooling) to the electrical energy consumed. In heating mode (Fig. 22a), the COP generally remains high (above 6.5) during early hours when the outdoor temperature is relatively stable (see the yellow trace in Fig. 20a). This indicates an efficient operation under moderate heating loads. However, a slight drop in COP is observed around 08:00, coinciding with the peak heat demand due to the simultaneous need for space heating and DHW. This drop can be attributed to the HP operating closer to its capacity limit, where efficiency is often reduced, or due to the elevated thermal lift caused by a large temperature gradient between the supply and return flow. Essentially, the HP operates more efficiently when it works against a smaller temperature gradient. Following this period, the COP stabilises at approximately 6.0 for the rest of the day and the system operates in a steady-state condition.

For the hot summer day (Fig. 22b), the COP remains relatively higher compared to the winter scenario, staying above 7.0 for most of the day. This reflects the inherently higher efficiency of the HP in cooling mode, as the thermal lift is smaller due to a closer alignment between indoor and outdoor temperatures. Slight fluctuations in COP can be seen between 09:00 and 18:00, coinciding with the rising outdoor temperature and increased cooling demand, as previously discussed. A peak in COP just after 23:00 aligns with the drop in cooling load during the evening hours, indicating the HP's ability to operate more efficiently under reduced thermal demand.

The auxiliary energy input to the storage tanks used for DHW (HWT-1) and space heating (HWT-2) is illustrated in Fig. 23. These inputs play a critical role in ensuring consistent hot water supply, especially during periods when the HP is either unable to fully meet the heating demand or is operating in cooling mode.

On the cold day in January, as shown in Fig. 23a, a notable difference is observed in the auxiliary energy usage between HWT-1 and HWT-2. The auxiliary heater for HWT-1 supplied a peak energy input of 0.56 kWh, while HWT-2 required no auxiliary input for space heating. This difference is primarily due to the operational mode of the HP during cold conditions. The HP caters to both space heating and DHW demands, but it prioritises space heating over DHW during periods of peak demand. As

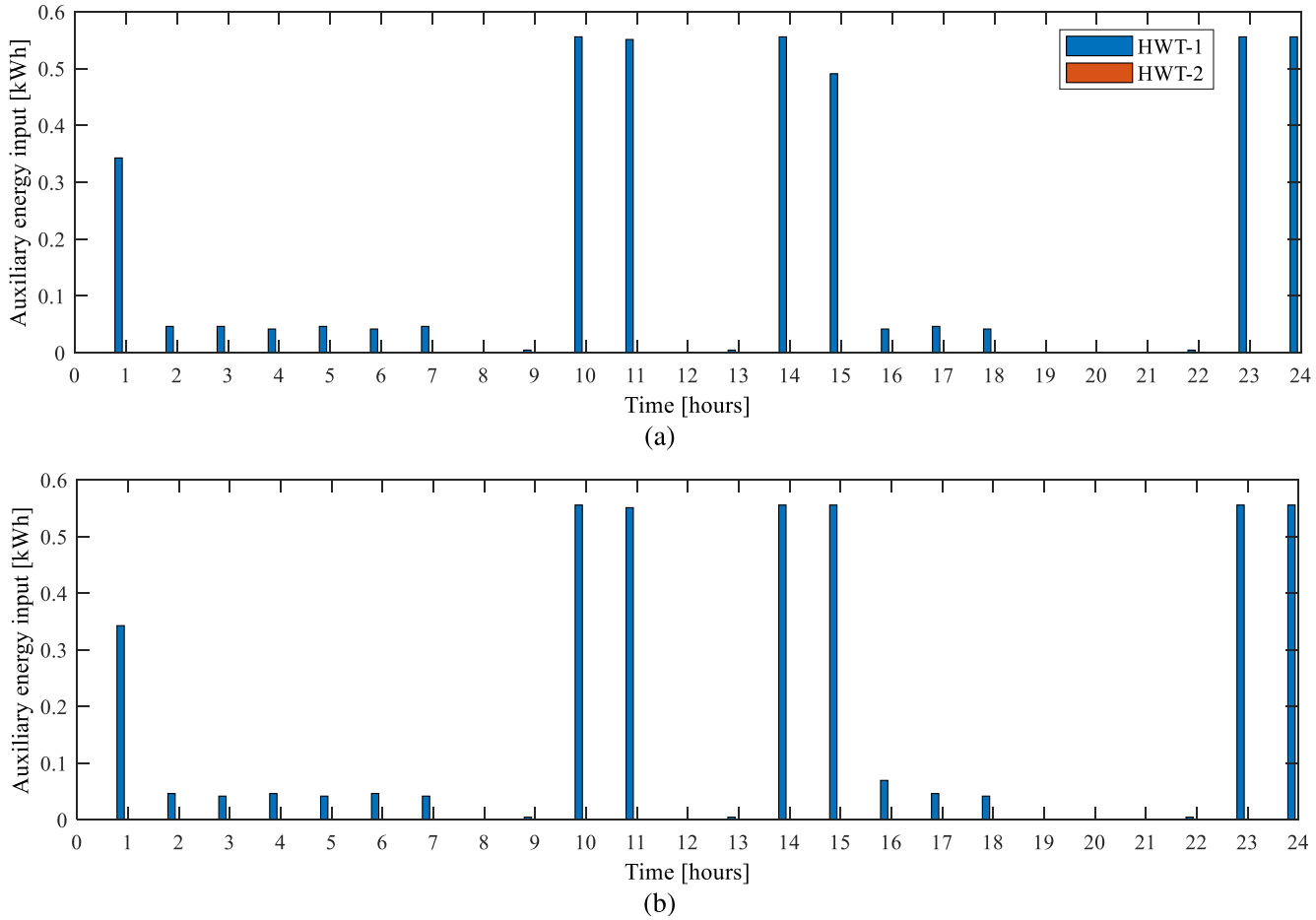

Fig. 23. Auxiliary energy input to DHW and space heating tanks on a) 15th January and b) 13th August.

a result, the auxiliary system is more heavily relied upon to maintain the DHW supply than for space heating. A simultaneous space heating and DHW load places an increased thermal demand on the HP, necessitating greater auxiliary support to compensate for DHW requirements.

In contrast, during the hot summer day in August, the HP operates solely in space cooling mode and does not contribute to the DHW supply. Consequently, all DHW requirements are met by the auxiliary heater in HWT-1. This results in intermittent but significant peaks in auxiliary energy input, as shown in Fig. 23b. The pronounced peak of 0.56 kWh at 15:00 compared to the winter day underscores the complete reliance of energy system on auxiliary heating for DHW when the HP is engaged in cooling mode.

The results in Fig. 23 demonstrate that the auxiliary heating requirements are influenced by the operational mode of the HP and seasonal temperature variations. During winter, the HP effectively meets space heating demand, diminishing the need for auxiliary energy input for HWT-2. This highlights the HP's robust thermal performance in challenging ambient temperatures. However, the demand for DHW remains consistent throughout the year, dictated by regular household consumption pattern and cold-water inlet temperature. The auxiliary system for HWT-1 exhibits a lower energy input during winter compared to summer. As previously mentioned, during simultaneous space heating and DHW demand, space heating is prioritised by the HP and the auxiliary system compensates for any shortfall in DHW supply. This highlights the role of the auxiliary heater in maintaining uninterrupted DHW supply during periods of high thermal demand or when the HP's capacity is stretched. The studied scenarios thus illustrate the importance of understanding the interplay between HP operation, auxiliary heating, and seasonal variations in optimising the energy performance of integrated space heating and DHW systems.

Fig. 24 shows a comparison of the monthly energy consumption by the boiler and HP throughout the year based on historical weather data for 2022. As expected in the cold-dominated climate of the UK, the boiler's energy consumption peaks during the winter months, driven by the increased demand for space heating. In contrast, the energy consumption pattern of the HP exhibits a different seasonal trend, with the highest usage occurring during the summer months of July and August, reflecting elevated space cooling demand. This is followed by secondary peaks during the colder months of December and January.

Fig. 24 further highlights the significant difference in energy consumption of the two energy systems during winter. In January, the boiler consumed 349.3 kWh, whereas the HP required substantially less energy at only 156.7 kWh—approximately 2.2 times lower. This marked reduction in energy usage by the HP can be attributed to its high COP, which in turn ensures greater efficiency and lower energy loss. The energy consumption between the two configurations also differs significantly during summer. The boiler, responsible for DHW production only during this period, recorded an average monthly consumption of 264.7 kWh in July and August. In contrast, the HP configuration consumed around 230 kWh during each month to meet a combined demand of space cooling and DHW supply. This demonstrates that even during the summer, when the HP operates in cooling mode, its energy consumption remains lower than that of the boiler configuration even when the boiler does not provide cooling services.

The results presented in this section elucidate the efficiency advantages of the HP over the boiler. While the boiler exhibits a higher energy consumption during peak heating months, the HP achieves consistent energy savings throughout the year, highlighting its versatility in managing both heating and cooling demand effectively.

4.3. *Effect of internal heat gains*

Understanding the impact of internal heat gains on the space heating and cooling needs is vital for the accurate design of an energy system. In the literature many references assume the effects of these gains as negligible. However, not considering internal heat gains may lead to designs susceptible to overheating or undercooling of thermal zones. This is because incorporating these heat gains into the building thermal model raises indoor temperatures. While such an effect may have a positive impact during winter, an adverse effect may take place during summer. In winter, internal heat gains may reduce the amount of energy that needs to be supplied to the building envelope to maintain a certain level of thermal comfort. In contrast, in summer, the energy system may be required to remove the extra heat contributed by the internal heat gains.

Fig. 25 shows the variation in monthly energy consumption of the HP-based energy system with and without internal heat gains considered. As shown, these gains have opposing effects depending on the

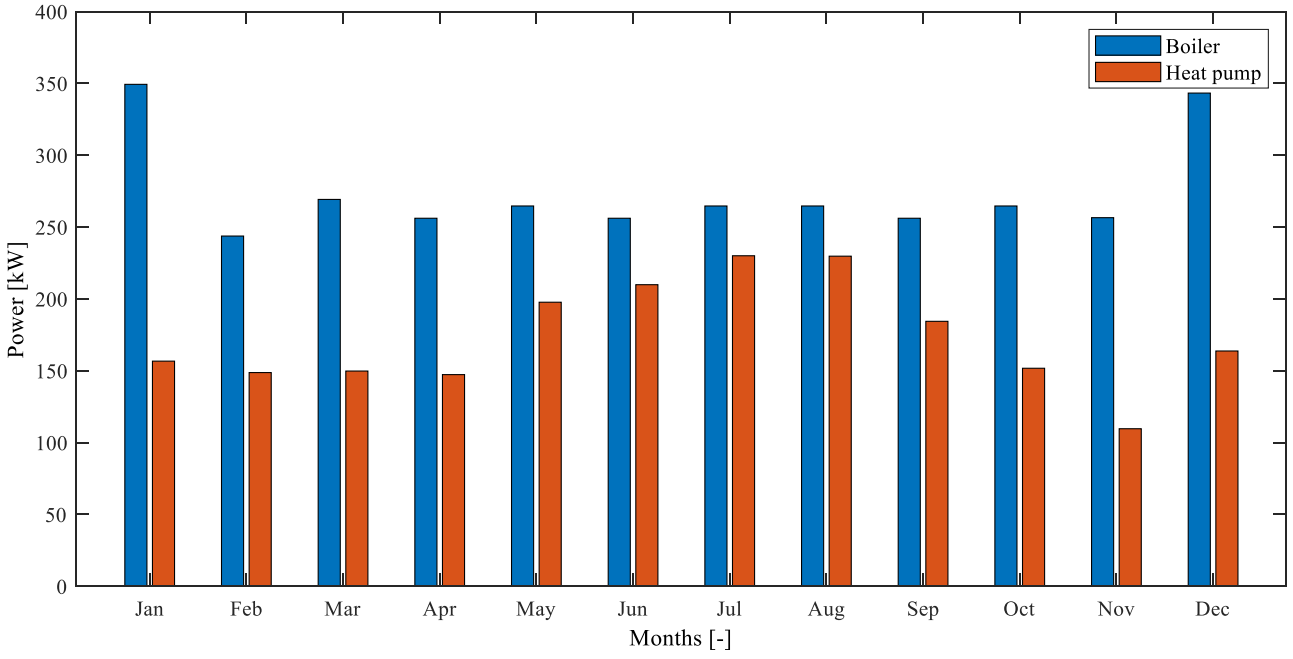

Fig. 24. Monthly energy consumption by HP vs boiler configuration.

season. In winter months, the influence of internal heat gains is relatively modest but still noteworthy as they lead to a reduction in energy consumption and an enhancement of system performance. For instance, energy consumption in January marginally decreased by ~1.84 kWh when internal heat gains were considered, but a substantial reduction of 44 kWh was observed in November. These reductions can be attributed to the additional heating provided by internal sources such as occupants, appliances, and lighting. The supplemental heat helps to maintain thermal comfort levels indoors, thereby reducing the heating load on the HP and improving energy efficiency during the cold season.

The impact of internal heat gains becomes more pronounced during summer and a notable increase in energy consumption is observed compared to when they are ignored. For instance, energy consumption rises by 55 % in July, followed by increases of 52 % in August, 41 % in June, 35 % in September, and 24 % in May. Such a significant rise can be attributed to the higher cooling demand resulting from the internal heat gains, which exacerbate the thermal load on the HP. The trend aligns with the elevated summer temperatures experienced during 2022 and shows how internal heat gains negatively affect system performance during the cooling season.

Fig. 26 presents the energy consumption of the boiler-based system, comparing scenarios with and without internal heat gains accounted for in the building model. The trends show that incorporating internal heat gains leads to significant reductions in overall energy consumption, particularly during the winter months. These reductions are primarily attributed to the supplementary heating provided by internal sources such as occupants, appliances, and lighting, which alleviate the boiler's operational load. During winter, the energy-saving impact of internal heat gains is pronounced, with reductions of ~50 % observed in November, December, January, and February. These substantial reductions reflect the critical role internal heat gains play in offsetting space heating demands. Unlike the HP, the boiler operates less efficiently when handling heating loads due to its reliance on direct combustion, which inherently involves higher energy losses. This aspect amplifies the relative energy savings achieved when internal heat gains are included, highlighting their importance in boiler-based systems.

In summer, the effect of internal heat gains on energy consumption is significantly lower but still evident. Energy consumption decreases by 13.2 kWh in June, 11.5 kWh in July and August, and a notable 62.8 kWh in September. These savings are lower than those observed during winter because in the summer the boiler is only responsible for DHW production and does not contribute to space cooling. The absence of cooling demand limits the influence of internal heat gains during warmer months.

The results presented in this section show that the impact of internal heat gains is more pronounced in the boiler-based system (Fig. 26) compared to the HP-based system (Fig. 25). This is largely because the boiler's efficiency remains constant irrespective of seasonal thermal demand, whereas the HP benefits from a (variable yet) high COP, which dynamically improves based on the thermal gradient. Therefore, the HP system is inherently better at integrating internal gains more effectively and overall operates more efficiently.

In general, from the results presented in Sections 4.1 to 4.3, the HP-based energy system is more energy efficient compared to the boiler-based system. In addition, a HP supported system offers the versatility of meeting both heating and cooling needs—a capability absent in boiler-based energy system. This dual functionality positions the HP as a more sustainable and flexible solution for year-round energy management.

4.4. Operational costs analysis

A cost comparison of meeting heat and cooling load by the boiler and HP-based configurations is shown in Fig. 27. Costs were calculated based on fixed tariffs for electricity (£0.43975/kWh), gas (£0.135/kWh), and a standing charge (£0.6236 per day). The energy consumed by the boiler was multiplied by the gas tariff, while the HP system costs were determined by multiplying electricity consumption by the corresponding tariff, also accounting for auxiliary heaters connected to the storage tanks. The standing charges were added to the cost of running both energy systems.

The results in Fig. 27 indicate that the HP configuration is consistently more expensive to operate throughout the year compared to the gas boiler-based system. On a monthly basis, this cost difference varies from £13.6 in November to £65.4 in July. The cumulative yearly cost of operating the HP system is approximately 1.7 times higher than the boiler-based system. The increased HP cost is evident during the summer months of July and August, where cooling demand adds to the system's

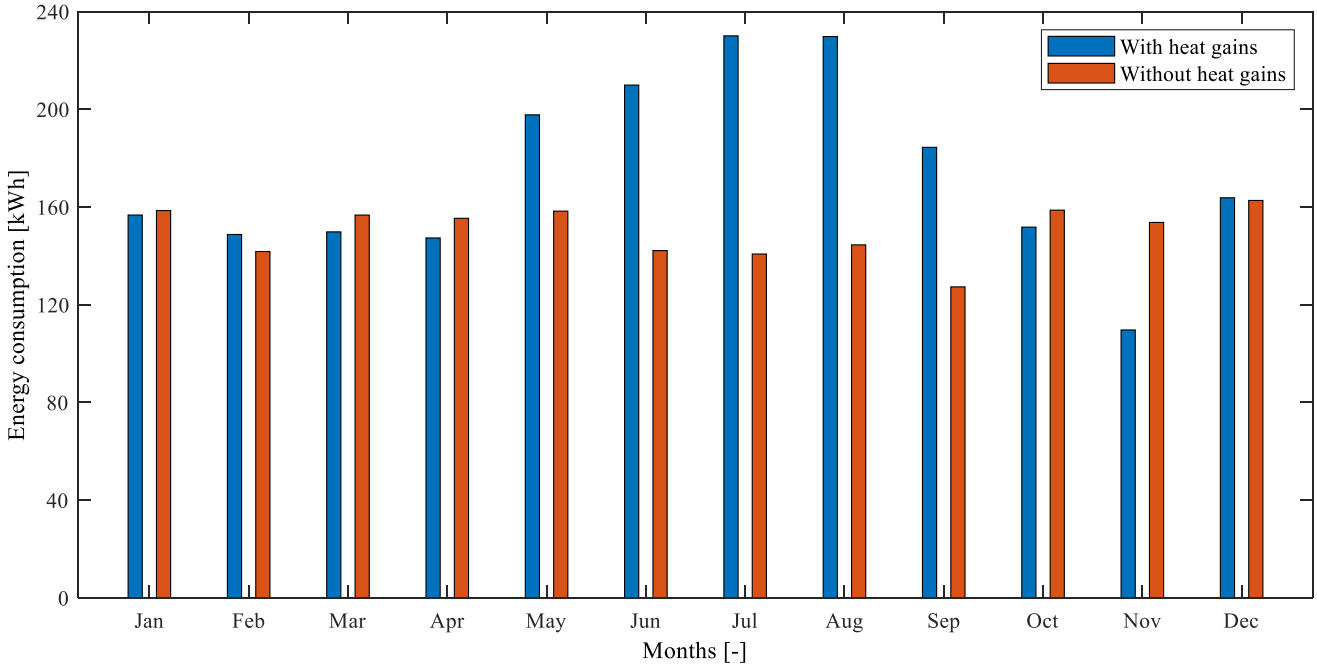

Fig. 25. Monthly energy consumption in HP-based configuration with and without internal heat gains.

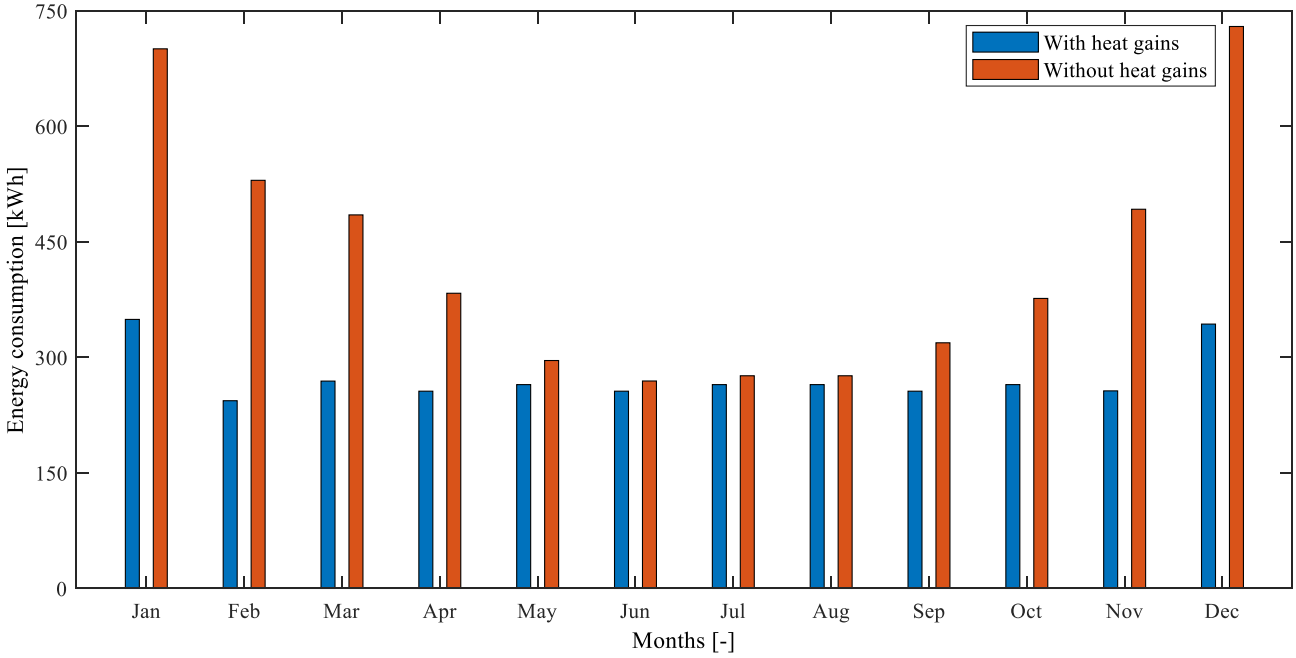

Fig. 26. Monthly energy consumption in boiler configuration with and without internal heat gains for 2022.

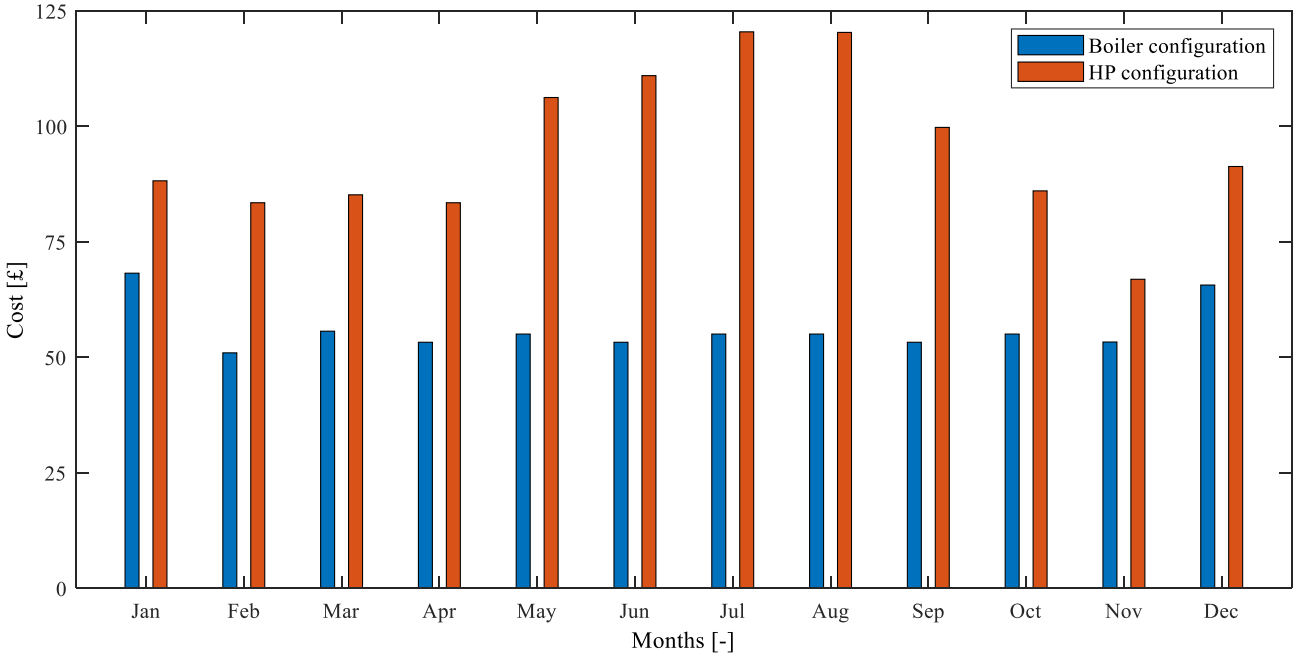

Fig. 27. Cost comparison between boiler and HP configuration.

energy consumption. In contrast, the boiler configuration incurs lower operational costs in summer as it is only responsible for meeting DHW requirements.

The higher operational costs for the HP system stem from a tariff structure that favours gas over electricity. Despite the HP's inherently higher efficiency, which theoretically reduces the required energy input, the disparity in energy costs offsets this gain. In contrast, the boiler configuration benefits from a significantly lower fuel cost for its operation. This underscores the impact of energy pricing policies on the economic viability of energy systems. If electricity prices were adjusted to be more competitive, the cost-benefit of HP systems would improve significantly, aligning their environmental sustainability and operational advantages with economic incentives. Such changes would potentially a) encourage a wider adoption of HP technologies in countries like the UK where heat demand is substantial, b) support the transition to more sustainable technologies, c) reduce carbon emissions, and d) ensure affordability for consumers.

4.5. *Extreme weather conditions*

Investigating the performance of an energy system under future weather conditions is important to assess system behaviour and understand the effect of future thermal loads on the housing stock. Climate data of 20 years with one hour resolution from UKCP [61] were assessed

to determine extreme weather conditions from 2021 to 2040. The number of hot and cold instances in each year were obtained within this period. These were identified using the heating and cooling setpoints defined by CIBSE Guide A [43].

The total yearly extreme weather occurrences for the time period under consideration are shown in Fig. 28. The highest number of cold instances take place in 2024 (a total of 7274), while the highest number of hot instances are seen in 2025 (a total of 833). Due to this, years 2024 and 2025 were selected to be further examined. An interesting pattern is observed in Fig. 28. A drastic zig-zag behaviour for these two years is exhibited, which could be attributed to the effects of El Niño and La Niña. These weather phenomena may lead to an excessively cold winter in 2024 and severe heatwaves in 2025. In the past, the risk of an increase of colder winters in the UK has been attributed to the presence of El Niño [62].

Fig. 29 shows the monthly heating and cooling demand for the energy system utilising a HP for years 2024 and 2025. These results account for internal heat gains due to occupancy, lighting, and equipment as outlined in Section 2.2. To aid the interpretation of results, the figure also shows the outdoor temperature throughout the two years with a black trace. The data reveal clear seasonal variations in heating and cooling loads, with notable increases compared to year 2022 (assessed in previous sections of the paper), reflecting evolving weather patterns and climate variability.

The heating load during the winter months of 2024 is marginally higher compared to the 2022 scenario discussed in Section 4.3. Specifically, the heating demand increases by 31 % in November, 2 % in December, 9 % in January, and 2 % in February. These increases point to colder winter conditions in 2024 relative to 2022, highlighting the influence of reduced ambient temperature on heating requirements.

Similarly, the cooling demand for 2025 also shows a marked increase compared to 2022, which was characterised by significant cooling loads due to unusually high ambient temperature. The cooling demand is 16 % higher in June, 10 % higher in July, and 22 % higher in September. Cooling requirements for 2025 span from May to October, with a peak demand of 806 kWh in July, followed by 710 kWh in August, 696 kWh in June, 531 kWh in September, and 496 kWh in May. These values indicate an extended cooling season, driven by prolonged periods of elevated outdoor temperatures—evidenced by the black trace in Fig. 29. This trend aligns with predictions of climate change impacts, with rising global temperatures resulting in more frequent and intense heatwaves. The growing cooling demand highlights the critical need for energy systems to adapt to extended periods of thermal stress.

Despite the greater number of cold instances in 2024 (7274 compared to 6293 in 2025), the heating load in early 2025 is still higher, particularly in January and March. This discrepancy is primarily because the temperatures in some days of 2025 drop significantly lower than the equivalent cold days in 2024, resulting in greater energy demand to maintain thermal comfort. In contrast, cooling requirements during the summer of 2024 are relatively lower than in 2025. However, with more frequent and intense heatwaves predicted in future years, cooling demand is expected to increase substantially. In this case, demand peaks in July 2025, reflecting the prolonged and intensified summer heat. Such a growing demand for space cooling exemplifies the dual challenge of managing both heating and cooling loads in future energy systems.

The energy consumption under forecasted weather conditions for July and August 2025 was assessed in further detail, with relevant information shown in Fig. 30. These results show distinct patterns in thermal demand. In July (Fig. 30a), the cooling load (blue bars) gradually increases throughout the month and peaks towards the end. The total cooling load for July is 806 kWh, accounting for approximately 86 % of the total energy load met by the HP. In contrast, the heating load (red bars) remains relatively steady throughout. This is because it exclusively reflects the DHW demand given there are no space heating requirements during July. The total heating load for July is 131 kWh, representing the remaining 14 % of the total energy load.

A similar trend is observed for the heating load in August (Fig. 30b), which increased slightly to 150 kWh—representing a 14.5 % rise compared to July. This increment is attributed to some space heating demand towards the end of the month as the ambient temperature decreases (black trace). Conversely, the cooling load reduced to 710 kWh in August—an 11.8 % reduction compared to July. Such a reduction reflects a slight easing of cooling needs. The contrasting trends between July and August highlight the dynamic nature of thermal demand. While cooling dominates energy consumption, the consistent DHW-related heating load indicates its year-round presence. The distribution of energy loads between cooling and heating also reinforces the critical role of HP systems in addressing both demands efficiently, particularly in climates experiencing prolonged and intensified summer conditions.

4.6. A further insight into internal heat gain patterns

All simulation results presented so far have been obtained considering the internal heat gain profiles presented in Section 2.2 in Fig. 5. These were based on [42], which was designed to assess building design to mitigate overheating risks. Lengthy occupancy patterns have been assumed, which is arguably unrealistic. To incorporate more realistic

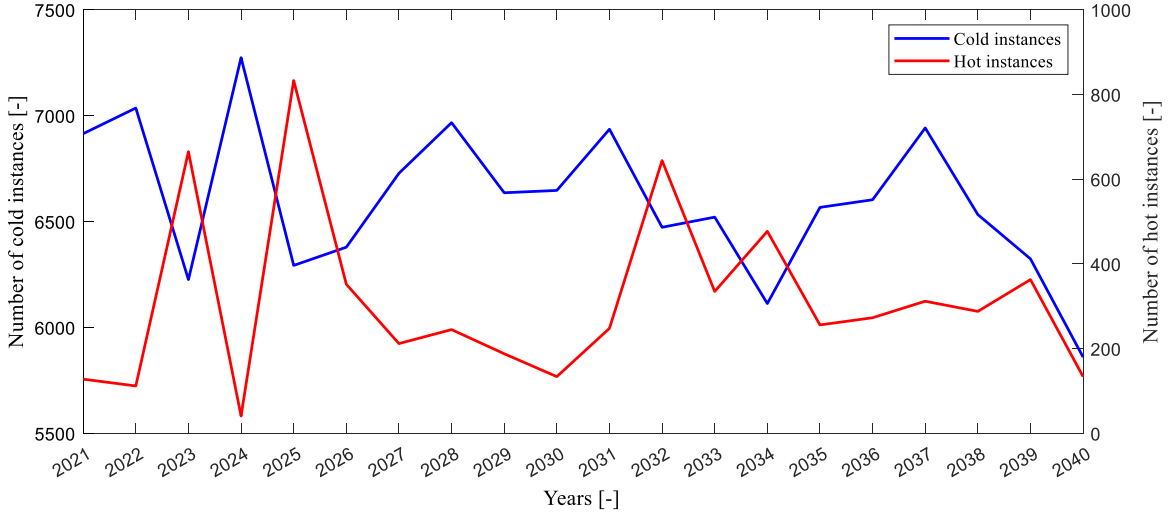

Fig. 28. Highest number of cold and hot instances in years 2021 to 2040.

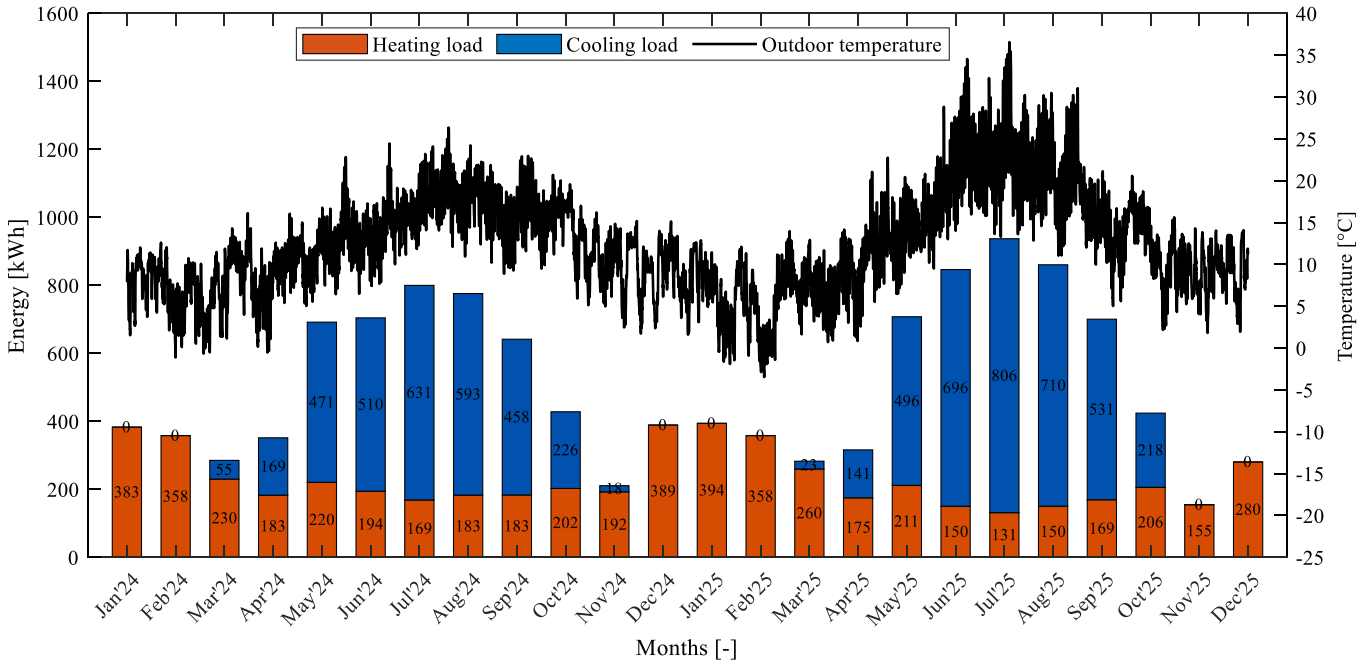

Fig. 29. Energy load met by the HP-based energy system under extreme weather conditions.

patterns, internal heat gains were modelled using ISO-recommended profiles for occupants, appliances, and lighting in residential houses per unit floor area. These profiles were scaled by multiplying the heat gains with the floor area as provided by [63]. Different hourly profiles for internal heat gains were used for weekdays and the weekend. These are summarised in Table 8.

The monthly energy consumption of the house was compared for two scenarios: one based on the heat gain profiles from CIBSE TM59 and the other based on ISO standards. Results are provided in Fig. 31. A HP-based configuration was considered in both cases. The outdoor temperature profile for year 2022 shown in Fig. 2 was adopted.

As observed in Fig. 31, the energy consumption between the two scenarios varies significantly throughout the year, highlighting the influence of internal heat gain assumptions on thermal demand. During the intermediate months of March, April, October and November, the energy consumption is lower for the CIBSE scenario compared to the ISO profiles. This difference is attributed to the higher internal heat gains accounted for in the CIBSE profiles, which effectively reduce the need for heating. However, a higher cooling demand is observed in the warmer months (including all summer, from May to September) when the CIBSE profiles are adopted. This is due to the increased heat contribution from internal sources and the corresponding rise in indoor temperature — in turn leading to additional cooling requirements to maintain thermal comfort. This warmer period of the year showcases the most notable differences in energy consumption compared to the simulation conducted with ISO profiles.

Energy consumption is also slightly lower for the ISO profiles compared to the CIBSE profiles during the winter months of December, January, and February. Although CIBSE profiles include higher internal heat gains, these may not be evenly distributed or may occur during times when the heat is not as effectively utilised for offsetting heating demand. For instance, if the internal heat gains occur during periods when the space is already warm, they may not contribute to reducing the heating load. Conversely, the ISO gains might coincide better with the periods of highest heat demand, resulting in a more effective use of internal heat to reduce the thermal load. On average, the weekly internal heat gains calculated using ISO profiles are ~3.8 times lower than those derived from CIBSE TM59. This substantial difference explains the lower energy consumption in the ISO scenario for the summer months and the reduced heating demand in the CIBSE scenario during the intermediate months.

5. Limitations of the work

While the studies conducted in this paper provide valuable insights into the performance of integrated heating and cooling systems, it is important to acknowledge some limitations. These limitations, arising from assumptions and simplifications in the modelling approach, may influence the general applicability of the research methodology and findings.

Firstly, the internal heat gains and usage patterns for occupancy, lighting, and equipment are based on the CIBSE TM59 standard, which is tailored for the UK context. Therefore, these values may not be directly applicable to other regions of the world with different building regulations, climate conditions, and occupancy behaviours. For accurate estimation of thermal energy demand in other locations, it is necessary to use internal heat gain values and usage patterns consistent with local standards.

Shading effects from external elements such as trees or from internal interventions like blinds or curtains have not been considered in this study. Additionally, windows were assumed to remain closed at all times to simplify the modelling. These simplifications may have slightly overpredicted the thermal energy demand of the house.

With regards to the water-to-water HP system adopted in this work, the source-side ground heat exchanger was not explicitly modelled in TRNSYS to simplify the simulation. This assumption was made as ground heat exchangers can provide water at a relatively stable temperature throughout the year. Therefore, a constant water temperature was assumed on the source-side of the heat pump.

Furthermore, in the simulation model separate hot water storage tanks for space heating and DHW were considered to streamline the implemented control strategy. However, these systems in practice are often integrated into a single enclosure or a single tank, where separate outlets for low-temperature space heating and high-temperature DHW supply are utilised. Modelling these systems as separate units may slightly influence system efficiency and control complexity.

As a final observation, the role of internal heat gains in the energy consumption of buildings requires further scrutiny. While these heat

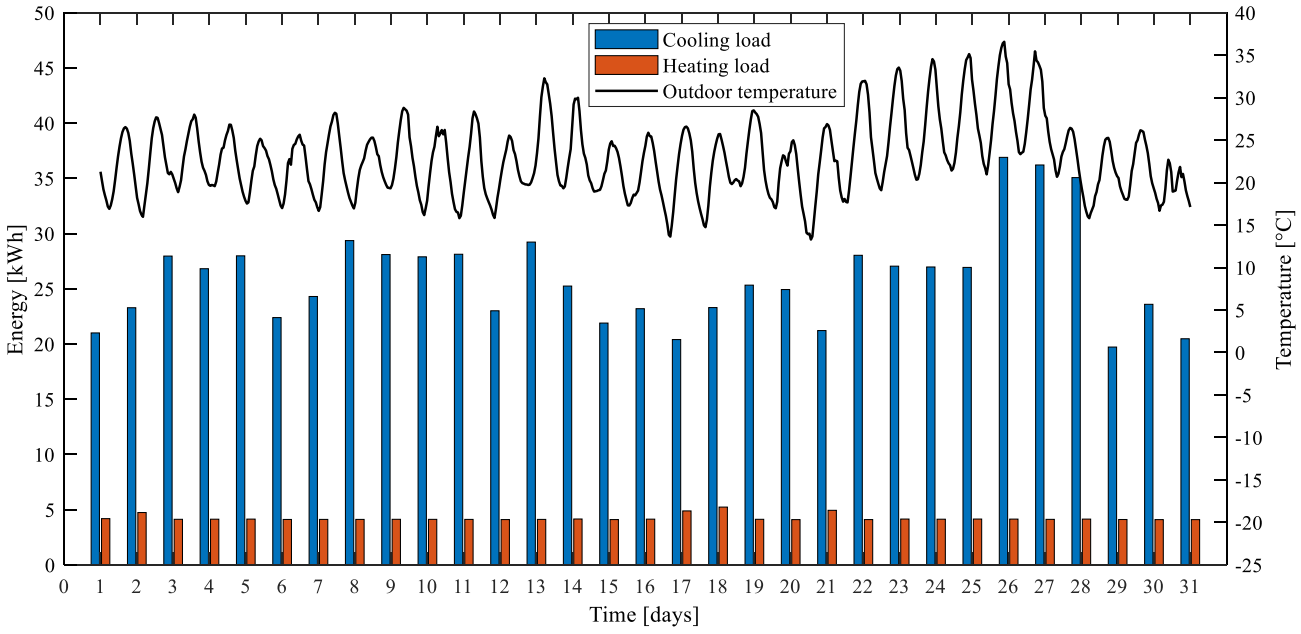

(a)

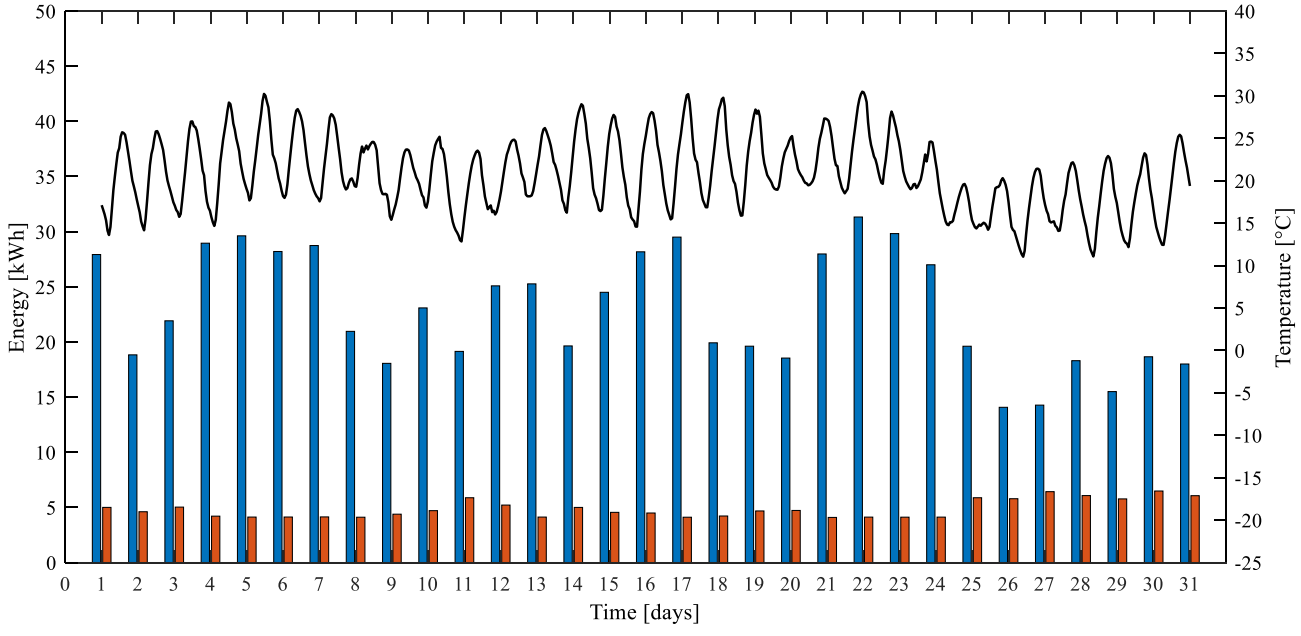

(b)

Fig. 30. Energy load met by HP configuration a) July 2025 and b) August 2025.

gains may result in energy savings during colder months, they may also lead to a reduced energy efficiency during warmer periods. These dynamics may shift in the future for traditionally cold-dominated countries like the UK, where rising ambient temperatures and more frequent and intense heatwaves due to global warming are expected. Such changes could further amplify the cooling demand during summer. To mitigate these challenges, ensure energy efficiency across seasons and balance the benefits and drawbacks of internal heat gains under evolving climatic conditions, adaptive strategies such as advanced control systems, dynamic insulation, and improved thermal zoning could be considered.

6. Conclusion

A detailed dynamic simulation of an energy system considering a TES-integrated reversible HP was presented in this paper. To accurately determine the thermal performance of the system, detailed three-dimensional modelling of a residential house based on a real building located in Cardiff, UK, was conducted. Internal heat gains due to occupancy, lighting, and electrical equipment were also incorporated along with their utility schedules into the building model according to UK building standards. The energy system was designed to meet space heating and space cooling requirements in addition to the year round demand for DHW. The performance of the reversible HP-based energy system was compared with a typical gas boiler energy system to

Table 8
ISO-17772 recommended profiles for internal heat gain.

Weekdays					Weekend days				
Time (hours)	Occupant (W/m^2)	Equipment Occupant (W/m^2)	Light Occupant (W/m^2)	Total gain (W)	Time (hours)	Occupant (W/m^2)	Equipment Occupant (W/m^2)	Light Occupant (W/m^2)	Total gain (W)
0	1.9	1.2	0	188.26	0	1.9	1.2	0	188.26
1	1.9	1.2	0	188.26	1	1.9	1.2	0	188.26
2	1.9	1.2	0	188.26	2	1.9	1.2	0	188.26
3	1.9	1.2	0	188.26	3	1.9	1.2	0	188.26
4	1.9	1.2	0	188.26	4	1.9	1.2	0	188.26
5	1.9	1.2	0	188.26	5	1.9	1.2	0	188.26
6	0.95	1.2	1.55	224.70	6	1.52	1.2	1.55	259.32
7	0.95	1.68	1.55	253.85	7	1.52	1.68	1.55	288.47
8	0.95	1.68	1.55	253.85	8	1.52	1.68	1.55	288.47
9	0.19	1.2	1.55	178.55	9	1.52	1.2	1.55	259.32
10	0.19	1.2	0.52	115.99	10	1.52	1.2	0.52	196.77
11	0.19	1.44	0.52	130.57	11	1.52	1.44	0.52	211.34
12	0.19	1.44	0.52	130.57	12	1.52	1.44	0.52	211.34
13	0.38	1.44	0.52	142.11	13	1.52	1.44	0.52	211.34
14	0.38	1.44	0.52	142.11	14	1.52	1.44	0.52	211.34
15	0.38	1.2	0.52	127.53	15	1.52	1.2	0.52	196.77
16	0.95	1.2	2.07	256.28	16	1.52	1.2	2.07	290.90
17	0.95	1.68	2.07	285.43	17	1.52	1.68	2.07	320.05
18	0.95	1.68	2.07	285.43	18	1.52	1.68	2.07	320.05
19	1.52	1.92	2.07	334.62	19	1.52	1.92	2.07	334.62
20	1.52	1.92	2.07	334.62	20	1.52	1.92	2.07	334.62
21	1.52	1.92	2.07	334.62	21	1.52	1.92	2.07	334.62
22	1.9	1.44	1.55	296.97	22	1.9	1.44	1.55	296.97
23	1.9	1.44	1.55	296.97	23	1.9	1.44	1.55	296.97

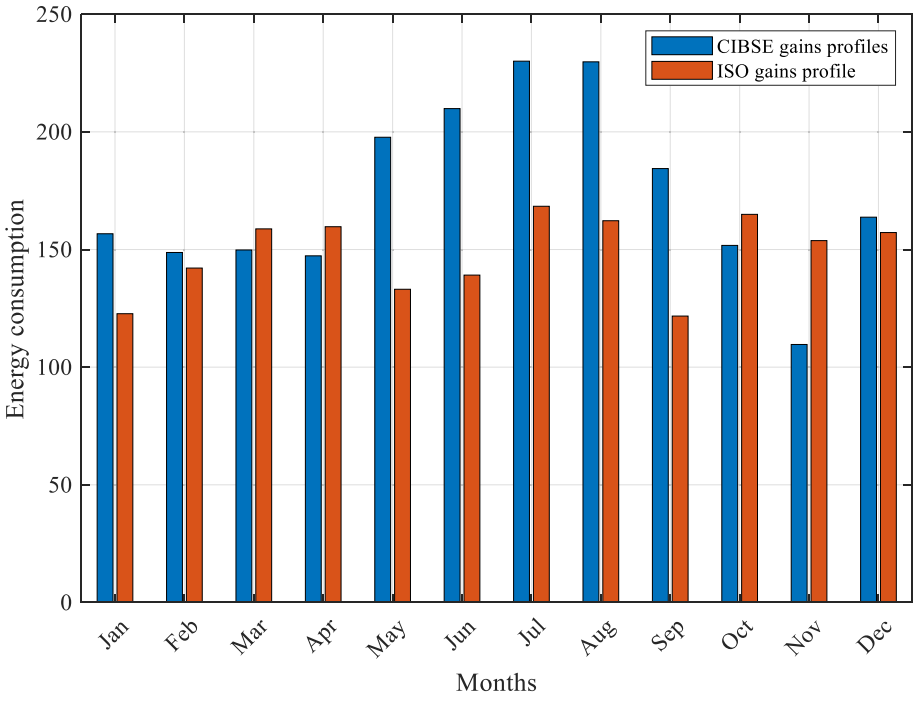

Fig. 31. Energy consumption of HP based energy system considering internal heat gain profiles from CIBSE and ISO.

investigate the challenges in replacing conventional heat provision systems. Furthermore, the performance of the HP-based energy system was evaluated under extreme weather conditions based on future climate projections.

The paper provides an initial framework to design a heat pump-based energy system and evaluate its performance to fulfil residential thermal demand. This approach could be used to inform building developers, utilities, and local authorities on heating/cooling demand peaks, overheating risks, and energy efficiency of typical UK dwellings in a warming world. The following conclusions are drawn from the present work:

- The multi-zone modelling approach adopted in this paper is suitable to design and study the performance of other types of residential dwellings (e.g. flats, semi-detached houses, fully-detached houses) and help sizing low-carbon technologies to meet heating and cooling demand. Such an approach is thus suitable to support the transition to net-zero.

- Energy consumption of the reversible HP-based system was significantly lower than for a conventional gas boiler-based system. For the system under study in this paper, the HP energy system consumes yearly around 1.58 times less energy than the gas boiler energy system.
- The impact of internal heat gains for accurate modelling of a thermal envelope of a building cannot be ignored. The yearly energy consumption with and without internal heat gains varied by 15.5 % for the HP-based system and 35.9 % in case of the gas boiler-based energy system.
- The cumulative yearly cost of operating the reversible HP-based energy system is approximately 1.7 times higher than for a conventional gas boiler-based energy system. These results must be interpreted with care as capital and installation costs were not considered in the calculations. Subsidies or appropriate mechanisms may be required to support electrification of heat to decarbonise the heating and cooling sector.
- Based on future climate projections, frequent, intense, and severe heatwaves are anticipated, which indicates an inevitable rise in space cooling demand. Therefore, in addition to replacing equipment contributing to greenhouse gas emissions with low-carbon and energy efficient technologies, special consideration must be given to cooling needs while supporting heat decarbonisation pathways.

CRediT authorship contribution statement

Arslan Saleem: Writing – review & editing, Writing – original draft, Visualization, Validation, Software, Methodology, Investigation, Formal analysis, Data curation, Conceptualization. **Carlos E. Ugalde-Loo:** Writing – review & editing, Writing – original draft, Supervision, Resources, Project administration, Investigation, Funding acquisition, Formal analysis.

Declaration of competing interest

The authors declare that they have no known competing financial interests or personal relationships that could have appeared to influence the work reported in this paper.

Acknowledgments

The work presented in this paper was supported by the Engineering and Physical Sciences Research Council (EPSRC), UK Research and Innovation, through the project 'Flexibility from Cooling and Storage (Flex-Cool-Store)' under grant EP/V042505/1. The authors would like to thank Mr. Lloyd Corcoran and Dr. Pranaynil Saikia for their support in conducting the software verification exercise. The authors also thank Dr. Ivan de la Cruz for his support in implementing the PI-based control strategies for the gas boiler and heat pump system configurations.

Appendix A

This Appendix provides an explanation of the mathematical equations and assumptions used for the components employed in the TRNSYS model of a dwelling.

A.1. THERMAL NODE / AIRNODE

Type56 (multi-zone building model) models the thermal behaviour of a building by dividing it into different thermal zones. The heat balance equation is solved for each zone/air-node as shown in the schematic provided in Fig. A1. To use this component, a separate pre-processing program must first be executed. A dynamic 3D-building simulation will be carried out by TRNSYS using the 3D drawing capabilities of Trnsys3d for Google Sketch-up, then importing the geometrical information into the Type56.

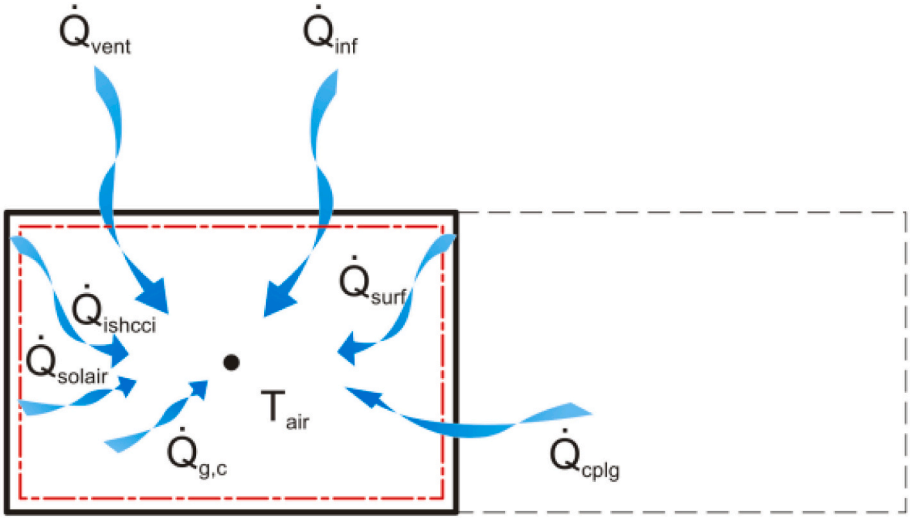

Fig. A1. Heat balance on the air node.

The convective heat flux to the air node is expressed as

$$\dot{Q}_i = \dot{Q}_{surf,i} + \dot{Q}_{inf,i} + \dot{Q}_{vent,i} + \dot{Q}_{g.c,i} + \dot{Q}_{cplg,i} + \dot{Q}_{solair,i} + \dot{Q}_{ISHCCI,i} \quad (A.1)$$

where index i denotes the i-th air node, $\dot{Q}_{surf,i}$ is the convective gain from surfaces. $\dot{Q}_{inf,i}$ stands for the infiltration gain (air flow from outside only),

given by

$$\dot{Q}_{inf,i} = \dot{V}\rho c_p\left(T_{outside,i} - T_{air}\right) \tag{A.2}$$

where $\dot{V}$ is the volumetric flow rate, ρ is the density, c_p is the specific heat, $T_{outside,i}$ is the temperature outside the air node, and T_{air} is the temperature of the air. $\dot{Q}_{vent,i}$ is the ventilation gain (air flow from a user-defined source, like an HVAC system), given by

$$\dot{Q}_{vent,i} = \dot{V}\rho c_p\left(T_{ventilation,i} - T_{air}\right) \tag{A.3}$$

where $T_{ventilation,i}$ is the ventilation temperature. $\dot{Q}_{g,c,i}$ is the internal convective gain (e.g. by people, equipment, illumination, radiators), and $\dot{Q}_{cplg,i}$ is the gain due to (connective) air flow from air node i or boundary condition, given by

$$\dot{Q}_{cplg,i} = \dot{V}\rho c_p\left(T_{zone,i} - T_{air}\right) \tag{A.4}$$

where $T_{zone,i}$ is zone temperature. $\dot{Q}_{solair,i}$ the fraction of solar radiation entering an airnode through external windows which is immediately transferred as a convective gain to the internal air, and $\dot{Q}_{ISHCCI,i}$ is the absorbed solar radiation on all internal shading devices of zone and directly transferred as a convective gain to the internal air.

A.2. Heat pump performance

The TRNSYS Tess Library [64] contains several HP models, mainly aimed at modelling air-to-air or air-to-water HPs. Some types, such as Type927 or Type1221, simulate the operating conditions of a water-to-water HPs—single-stage and two-stage, respectively.

The Type927 HP model utilises a performance map. This means its results are based on information contained in user-supplied data files containing catalogue data for the capacity and power draw as a function of entering load and source temperatures [65]. In the heating mode, Type927 calls the TRNSYS Data subroutine with the entering source and load fluid. The Data routine accesses the heating performance data file and returns the HP's heating capacity and power draw. The HP's COP in heating is given by:

$$COP = \frac{Cap_{heating}}{\dot{P}_{heating}} \tag{A.5}$$

where $Cap_{heating}$ is heating capacity of HP and $\dot{P}_{heating}$ is the power drawn by HP in heating mode.

The amount of energy absorbed from the source fluid stream in heating is given by:

$$\dot{Q}_{absorbed} = Cap_{heating} - \dot{P}_{heating} \tag{A.6}$$

The outlet temperatures of the two liquid streams can then be calculated using:

$$T_{source,out} = T_{source,in} - \frac{\dot{Q}_{absorbed}}{\dot{m}_{source}c_{p_{source}}} \tag{A.7}$$

where $T_{source,out}$ is the temperature of liquid exiting the source side of HP, $T_{source,in}$ is the temperature of liquid entering the source side of HP, $\dot{m}_{source}$ is mass flow rate of the liquid on the source side of HP, and $c_{p_{source}}$ is specific heat of the liquid on the source side of HP. For the load side,

$$T_{load,out} = T_{load,in} - \frac{Cap_{heating}}{\dot{m}_{load}c_{p_{load}}} \tag{A.8}$$

where $T_{load,out}$ is the temperature of liquid exiting the load side of HP, $T_{load,in}$ is the temperature of liquid entering the load side of HP, $\dot{m}_{load}$ is mass flow rate of the liquid on the load side HP, and $c_{p_{load}}$ is specific heat of the liquid on the load side of HP.

In cooling mode, Type927 operates in much the same fashion as in heating mode. The Data routine accesses the cooling performance data file and returns the machine's cooling capacity and power draw. The HP's COP in cooling is given by:

$$COP = \frac{Cap_{cooling}}{\dot{P}_{cooling}} \tag{A.9}$$

where $Cap_{cooling}$ is cooling capacity of HP and $\dot{P}_{cooling}$ is the power drawn by HP in cooling mode.

The amount of energy rejected by the source fluid stream in cooling is given by:

$$\dot{Q}_{rejected} = Cap_{cooling} + \dot{P}_{cooling} \tag{A.10}$$

The outlet temperatures of the two liquid streams can then be calculated using

$$T_{source,out} = T_{source,in} + \frac{\dot{Q}_{rejected}}{\dot{m}_{source}c_{p_{source}}} \tag{A.11}$$

$$T_{load,out} = T_{load,in} + \frac{Cap_{cooling}}{\dot{m}_{load}c_{p_{load}}} \tag{A.12}$$

A.3. Storage tank

Heat is transferred into and out of the storage tank through two fluid streams that mix with the storage. This problem can be resolved by solving the differential equation:

$$\frac{dT_{tank}}{dt} = \frac{Q_{in,tank} - Q_{out,tank}}{C_{tank}} \tag{A.13}$$

The storage tank model allows for the designation of stratification levels by specifying a number of tank nodes N. The tank is divided into N horizontal nodes of equal size, each assumed to be isothermal. Node 1 is positioned at the top of the storage tank.

This model accounts for various heat transfers, including thermal losses to the environment through the top, sides, and bottom of the tank. It also considers conduction between adjacent nodes, mixing between nodes to eliminate thermal instabilities, mixing due to load flow through the tank, and auxiliary heat input.

The storage tank exchanges heat with its environment through losses or gains from the top, edges, and bottom areas. The model allows for the specification of unique environmental temperatures for the top, bottom, and edges, enhancing flexibility. The heat transfer for tank node (j) from these areas is:

$$Q_{loss,top,j} = A_{top,j} U_{top} \left(T_{tank,j} - T_{env,top}\right) \tag{A.14}$$

where, $Q_{loss,top,j}$ is the heat loss from the top of node, $A_{top,j}$ is the tank top surface area for thermal losses (all attributed to tank node 1), U_{top} is the storage tank top heat loss coefficient and $T_{env,top}$ is tank environment temperature for losses through the top of the storage. The subscripts 'bottom' and 'edges' refer to the parameters corresponding to bottom and edges of the tank. The respective equations are:

$$Q_{loss,bottom,j} = A_{bottom,j} U_{bottom} \left(T_{tank,j} - T_{env,bottom}\right) \tag{A.15}$$

$$Q_{loss,edges,j} = A_{edges,j} U_{edges} \left(T_{tank,j} - T_{env,edges}\right) \tag{A.16}$$

The nodes in the storage tank can interact thermally via conduction between nodes. The formulation of the conductivity heat transfer from tank node j (is)

$$Q_{cond,j} = k_j A_j \frac{T_j - T_{j+1}}{L_{cond,j}} + k_{j-1} A_{j-1} \frac{T_j - T_{j-1}}{L_{cond,j-1}} \tag{A.17}$$

where k_j is the thermal conductivity of fluid in node j, A_j is the conduction interface area between this node and the one below it and A_{j-1} is the conduction interface area between this node and the one above it, T_j denotes temperature of jth node, T_{j+1} and T_{j-1} are the tempertures of the nodes directly below and directly above the jth node, $L_{cond,j}$ represents vertical distance between the centroid of this node and the centroid of the node below, and $L_{cond,j-1}$ is the vertical distance between the centroid of this node and the centroid of the node above.

At times, the nodes in the storage tank may become thermally unstable (a node has a higher temperature than the node above). If this happens, the model completely mixes any nodes that are unstable at the end of the timestep to avoid problems.

The storage tank relies on external controls to add or remove heat, allowing for the modelling of auxiliary heating effects such as electrical elements or combustion heating. Users can input heat rates for each node in the tank through the model. For instance, an aquastat model might detect the temperature at the top node and send a control signal to an auxiliary heater, which then adds heat to the bottom node until the top node reaches its setpoint. Once this setpoint is achieved, the aquastat disables the control signal, stopping the heat input.

The differential equations for the tank nodes can be written as:

$$\frac{dT_{tank,j}}{dt} = \frac{Q_{in,tank,j} - Q_{out,tank,j}}{C_{tank,j}} \tag{A.18}$$

where $Q_{in,tank}$ and $Q_{out,tank}$ are functions of the ambient temperature and the inlet fluid conditions and flow rates. $T_{tank,j}$ is the temperature of the tank node, and C_{tank} is the capacitance of the tank.

The coupled differential equations are solved using an approximate analytical method. While this solution is independent of the timestep, it requires an iterative process within the subroutine to resolve the equations. The above equation can be expanded to:

$$\frac{dT_{tank,j}}{dt} = \frac{Q_{aux,j} - Q_{loss,top,j} - Q_{loss,bottom,j} - Q_{loss,edges,j} - Q_{cond,j} - Q_{flow,i,j} - Q_{mix,j}}{C_{tank,j}} \tag{A.19}$$

These equations are then placed in the form:

$$\frac{dT}{dt} = aT + b \tag{A.20}$$

where T is the dependent variable, t is time, a is a constant and b may be a function of time or the dependent variable. If b is a constant, than the solution of this differential equation can be readily solved. If b is not constant, then a reasonable approximation to the analytical solution can be found by assuming that b is constant over the timestep and equal to its average value over the timestep.

At any time (for a not equal to zero):

$$T_{final} = \left(T_{initial} + \frac{b_{ave}}{a}\right) e^{a\Delta t} - \frac{b_{ave}}{a} \tag{A.21}$$

where

$$b_{ave} = b(T_{ave}) \tag{A.22}$$

and

$$T_{ave} = \frac{1}{a\Delta t}\left(T_{inital} + \frac{b_{ave}}{a}\right)(e^{a\Delta t} - 1) - \frac{b_{ave}}{a} \tag{A.23}$$

The values of a and b are found for each node. Term b holds the temperatures of other tank nodes. Temperatures in b are assumed to be constant for the solution of the nodal differential equations at their average value over the timestep. The nodal differential equation is then solved, new final and average nodal temperatures are calculated and the entire process is repeated until a converged solution is obtained.

A.4. Boiler

Type700 uses a simple efficiency equation to predict the energy required to heat a liquid to its setpoint temperature. The heater is capacity-limited, making it similar to the standard TRNSYS Type6. However, Type700 differs by also considering combustion efficiency, reporting energy lost during combustion and energy exhausted from the boiler stack.

If there is no liquid flow through the Type700 boiler, the model sets the output temperature and flow rate to match the input values. It also sets the energy transferred to the fluid, energy lost during combustion, energy exhausted through the stack, fuel consumption, and part load ratio to zero. This no-flow condition overrides the control signal, meaning the boiler can be 'ON' (control signal set to 1) but not meet the setpoint temperature if the input flow rate is zero.

When there is liquid flow but the control signal is 'OFF', the model sets the output temperature and flow rate to match the input values, and similarly sets all energy and fuel metrics to zero. If there is liquid flow and the control signal is 'ON', the model first calculates the energy required to raise the liquid temperature from its inlet value to the setpoint using:

$$\dot{Q}_{need} = \dot{m}_{fluid} c_{p\,fluid}(T_{set} - T_{in}) \tag{A.24}$$

where, $\dot{m}_{fluid}$ is the mass flow rate and $c_{p\,fluid}$ is the specific heat of the fluid, T_{set} is the setpoint temperature and T_{in} is the temperature of inflow fluid.

The required energy input $\dot{Q}_{need}$ is limited by the device capacity (specified as a parameter) and cannot be negative. Therefore, if the inlet temperature exceeds the setpoint temperature and the boiler control signal is 'ON', the device will not calculate a negative value for $\dot{Q}_{need}$. If $\dot{Q}_{need}$ does not exceed the device capacity, the energy transferred to the liquid stream ($\dot{Q}_{fluid}$) is set equal to $\dot{Q}_{need}$. The device is internally controlled to deliver only the required amount of energy to the liquid stream. Consequently, the outlet temperature is set to the setpoint temperature, and the part load ratio (PLR) is adjusted accordingly.

$$PLR = \frac{\dot{Q}_{need}}{\dot{Q}_{max}} \tag{A.25}$$

where $\dot{Q}_{max}$ is the maximum device capacity.

If the boiler is capacity limited because the required energy exceeds device capacity, $\dot{Q}_{fluid}$ is set to $\dot{Q}_{max}$, the PLR is set to 1 and the outlet fluid temperature is set according to:

$$\dot{Q}_{fuel} = \frac{\dot{Q}_{fluid}}{\eta_{boiler}} \tag{A.26}$$

where η_{boiler} represents the boiler efficiency.

The energy exhausted from the device is given by:

$$\dot{Q}_{exhaust} = \dot{Q}_{fuel}(1 - \eta_{combustion}) \tag{A.27}$$

where $\eta_{combustion}$ represents the combustion efficiency.

And the energy lost during the combustion process is given by:

$$\dot{Q}_{loss} = \dot{Q}_{fuel} - \dot{Q}_{exhaust} \tag{A.28}$$

A.5. Heating coil model

A simple heating coil model was adapted to estimate performance without needing detailed geometric characteristics of the coil. The model's parameters are solely the thermodynamic properties of the coil, requiring no specific manufacturer data. Based on the assumption of a constant heat transfer coefficient (UA) for the coil regardless of inlet conditions, the simulation model calculates the coil design U-factor times Area (UA) values from the design conditions.

First the capacity rates of the air (C_{air}) and liquid streams (C_{liq}) are calculated.

$$C_{air} = \dot{m}_{air,rated}\left(c_{p\,air} + \omega_{in,rated} c_{p\,vap}\right) \tag{A.29}$$

$$C_{liq} = \dot{m}_{liq,rated} c_{p_{liq}} \tag{A.30}$$

where, $\dot{m}_{air,rated}$ and $\dot{m}_{liq,rated}$ are the rated mass flow rate of air and liquid streams, $c_{p_{air}}$ is the specific heat of air, $c_{p_{vap}}$ is the specific heat of vapor, $c_{p_{liq}}$ is the specific heat of liquid, and $\omega_{in,rated}$ is the design inlet air humidity ratio.

Then the model iterates to find a UA for the coil which provides the outlet air temperature such that

$$Q_{rated} = C_{air}\left(T_{out} - T_{in,rated}\right) \tag{A.31}$$

where, Q_{rated} is the rated capacity, C_{air} is the air capacitance, T_{out} is the outlet air temperature, and $T_{in,rated}$ is the design Inlet Fluid Temperature.

The UA value for the coil is calculated only once per simulation, and in this version of the simple heating coil model, the UA is considered constant regardless of the inlet conditions. During an iterative call, the component first checks for both air flow and liquid flow through the heating coil. If either flow is zero, the outlet conditions are set to match the inlet conditions, and the component exits. If both air flow and liquid flow are present, the component determines all inlet air and liquid properties before calculating the capacity rates:

$$C_{air} = \dot{m}_{air}\left(c_{p_{air}} + \omega_{in} c_{p_{vap}}\right) \tag{A.32}$$

$$C_{liq} = \dot{m}_{liq} c_{p_{liq}} \tag{A.33}$$

where $\dot{m}_{air}$ and $\dot{m}_{liq}$ denote air and liquid mass flow rates, $c_{p_{air}}$, $c_{p_{vap}}$, and $c_{p_{liq}}$ denote the specific heat of air, vapor and liquid. ω_{in} is the inlet air humidity ration.

The outlet temperatures are then calculated from the inlet conditions, the capacity rates, the UA for the coil, and the coil configuration. Since this is an air heating process, the outlet air humidity ratio equals the inlet air humidity ratio. The total energy added to the air stream is then determined.

$$Q_{total} = C_{air}\left(T_{air,in} - T_{air,out}\right) \tag{A.34}$$

Appendix B

This Appendix provides the thermal capacitances adopted in the building models.

Table 9
Thermal capacitance of different zones adopted in the building model.

Zone	Volume (m^3)	Air capacitance (kJ/K)	Zone capacitance (kJ/K)
Kitchen (Sp1)	28.17	33.80	338.01
Living room (Sp2)	53.15	63.78	637.83
Bedroom 3 (single, Sp5)	15.02	18.02	180.24
Bedroom 1 (double, Sp6)	24.43	29.32	293.19
Bedroom 2 (single, Sp7)	19.43	23.31	233.11

Data availability

Relevant datasets produced for this paper have been made available in the Cardiff University data repository at https://doi.org/10.17035/cardiff.28152629.

References

[1] International Energy Agency. Global energy review : CO2 emissions in 2021 global emissions rebound sharply to highest ever level international energy. 2021.
[2] Eurostat. Energy data 2020 edition. 2020.
[3] Lowe R, Chiu LF. Innovation in deep housing retrofit in the United Kingdom: the role of situated creativity in transforming practice. Energy Res Soc Sci 2020;63:101391. https://doi.org/10.1016/j.erss.2019.101391.
[4] Biswas K, Patel T, Shrestha S, Smith D, Desjarlais A. Whole building retrofit using vacuum insulation panels and energy performance analysis. Energ Buildings 2019:203. https://doi.org/10.1016/j.enbuild.2019.109430.
[5] Park JH, Yun BY, Chang SJ, Wi S, Jeon J, Kim S. Impact of a passive retrofit shading system on educational building to improve thermal comfort and energy consumption. Energ Buildings 2020:216. https://doi.org/10.1016/j.enbuild.2020.109930.
[6] Touchie MF, Pressnail KD. Evaluating a proposed retrofit measure for a multi-unit residential building which uses an air-source heat pump operating in an enclosed balcony space. Energ Buildings 2014;85:107–14. https://doi.org/10.1016/j.enbuild.2014.08.048.
[7] Carragher M, De Rosa M, Kathirgamanathan A, Finn DP. Investment analysis of gas-turbine combined heat and power systems for commercial buildings under different climatic and market scenarios. Energy Convers Manag 2019;183:35–49. https://doi.org/10.1016/j.enconman.2018.12.086.
[8] Rogeau A, Girard R, Abdelouadoud Y, Thorel M, Kariniotakis G. Joint optimization of building-envelope and heating-system retrofits at territory scale to enhance decision-aiding. Appl Energy 2020;264:114639. https://doi.org/10.1016/j.apenergy.2020.114639.
[9] Gaur AS, Fitiwi DZ, Curtis J. Heat pumps and our low-carbon future: a comprehensive review. Energy Res Soc Sci 2021;71:101764. https://doi.org/10.1016/j.erss.2020.101764.
[10] Capros P, Kannavou M, Evangelopoulou S, Petropoulos A, Siskos P, Tasios N, et al. Outlook of the EU energy system up to 2050: the case of scenarios prepared for European Commission's "clean energy for all Europeans" package using the PRIMES model. Energ Strat Rev 2018;22:255–63. https://doi.org/10.1016/j.esr.2018.06.009.
[11] Bordignon S, Emmi G, Zarrella A, De Carli M. Energy analysis of different configurations for a reversible ground source heat pump using a new flexible TRNSYS type. Appl Therm Eng 2021;197:117413. https://doi.org/10.1016/j.applthermaleng.2021.117413.
[12] Breembroek G, Eggen G. Retrofitting with heat pumps in buildings: survey Report HPC - AR9. vol. 20. 2001.
[13] Miara M, Günther D, Langner R, Helmling S, Wapler J. 10 years of heat pumps monitoring in Germany. Outcomes of several monitoring campaigns. From low-energy houses to un- retrofitted single-family dwellings. 12th IEA Heat Pump Conference11; 2017.
[14] Huchtemann K, Müller D. Evaluation of a field test with retrofit heat pumps. Build Environ 2012;53:100–6. https://doi.org/10.1016/j.buildenv.2012.01.013.
[15] Maivel M, Kurnitski J. Low temperature radiator heating distribution and emission efficiency in residential buildings. Energ Buildings 2014;69:224–36. https://doi.org/10.1016/j.enbuild.2013.10.030.

[16] Lauenburg P, Wollerstrand J. Adaptive control of radiator systems for a lowest possible district heating return temperature. Energ Buildings 2014;72:132–40. https://doi.org/10.1016/j.enbuild.2013.12.011.
[17] Østergaard DS, Svendsen S. Replacing critical radiators to increase the potential to use low-temperature district heating – a case study of 4 Danish single-family houses from the 1930s. Energy 2016;110:75–84. https://doi.org/10.1016/j.energy.2016.03.140.
[18] Jangsten M, Kensby J, Dalenbäck JO, Trüschel A. Survey of radiator temperatures in buildings supplied by district heating. Energy 2017;137:292–301. https://doi.org/10.1016/j.energy.2017.07.017.
[19] Hasan A, Kurnitski J, Jokiranta K. A combined low temperature water heating system consisting of radiators and floor heating. Energ Buildings 2009;41:470–9. https://doi.org/10.1016/j.enbuild.2008.11.016.
[20] Sarbu I, Sebarchievici C. A study of the performances of low-temperature heating systems. Energ Effic 2015;8:609–27. https://doi.org/10.1007/s12053-014-9312-4.
[21] Fraga C, Hollmuller P, Schneider S, Lachal B. Heat pump systems for multifamily buildings: potential and constraints of several heat sources for diverse building demands. Appl Energy 2018;225:1033–53. https://doi.org/10.1016/j.apenergy.2018.05.004.
[22] Maivel M, Kurnitski J. Heating system return temperature effect on heat pump performance. Energ Buildings 2015;94:71–9. https://doi.org/10.1016/j.enbuild.2015.02.048.
[23] Wang Q, Ploskić A, Song X, Holmberg S. Ventilation heat recovery jointed low-temperature heating in retrofitting - an investigation of energy conservation, environmental impacts and indoor air quality in Swedish multifamily houses. Energ Buildings 2016;121:250–64. https://doi.org/10.1016/j.enbuild.2016.02.050.
[24] Ionesi A, Jradi M, Thorsen JE, Veje CT. Simulation of an adaptive heat curve for automatic optimization of district heating installation. 14th International Conference of IBPSA - Building Simulation BS 2015 Conference Proceedings. 2015; 2015. p. 2117–24. https://doi.org/10.26868/25222708.2015.2823.
[25] Huchtemann K, Müller D. Simulation study on supply temperature optimization in domestic heat pump systems. Build Environ 2013;59:327–35. https://doi.org/10.1016/j.buildenv.2012.08.030.
[26] Tunzi M, Østergaard DS, Svendsen S, Boukhanouf R, Cooper E. Method to investigate and plan the application of low temperature district heating to existing hydraulic radiator systems in existing buildings. Energy 2016;113:413–21. https://doi.org/10.1016/j.energy.2016.07.033.
[27] Wang H, Bo S, Zhu C, Hua P, Xie Z, Xu C, et al. A zoned group control of indoor temperature based on MPC for a space heating building. Energy Convers Manag 2023;290:117196. https://doi.org/10.1016/j.enconman.2023.117196.
[28] Saffari M, Keogh D, De Rosa M, Finn DP. Technical and economic assessment of a hybrid heat pump system as an energy retrofit measure in a residential building. Energ Buildings 2023;295:113256. https://doi.org/10.1016/j.enbuild.2023.113256.
[29] Battaglia V, Vanoli L, Verde C, Nithiarasu P, Searle JR. Dynamic modelling of geothermal heat pump system coupled with positive-energy building. Energy 2023; 284:128557. https://doi.org/10.1016/j.energy.2023.128557.
[30] Aneli S, Arena R, Marco Tina G, Gagliano A. Improvement of energy self-sufficiency in residential buildings by using solar-assisted heat pumps and thermal and electrical storage. Sustain Energy Technol Assess 2023;60:103446. https://doi.org/10.1016/j.seta.2023.103446.
[31] Werner-Juszczuk AJ, Siuta-Olcha A. Assessment of the impact of setting the heating curve on reducing gas consumption in a residential building while ensuring thermal comfort. Journal of Building Engineering 2024;94:110032. https://doi.org/10.1016/j.jobe.2024.110032.
[32] Acar U, Kaska O. Performance assessments of ground source heat pump assisted by various solar panels to achieve zero energy buildings in cold climate conditions. Journal of Building Engineering 2024;96:110611. https://doi.org/10.1016/j.jobe.2024.110611.
[33] Ning H, Wang Z, Xu Y, Liang F. Thermal performance of solar ground source heat pump system for rural buildings in Chinese cold zone. Results in Engineering 2024; 23:102603. https://doi.org/10.1016/j.rineng.2024.102603.
[34] Ugalde-Loo CE. Are we prepared to cool down in a warming world? Oxford Energy Forum 2022:47–51.
[35] Grid National. Future energy scenarios. http://fes.nationalgrid.com/media/1243/ac-2050-v21.pdf; 2018.
[36] Khosravi F, Lowes R, Ugalde-Loo CE. Cooling is hotting up in the UK. Energy Policy 2023;174:113456. https://doi.org/10.1016/j.enpol.2023.113456.
[37] Klein SA, Beckman W, Mitchell J, Duffie J, Duffie N, Freeman T. TRNSYS 18: A transient system simulation program. USA: Madison; 2017.
[38] Safa AA, Fung AS, Kumar R. Heating and cooling performance characterisation of ground source heat pump system by testing and TRNSYS simulation. Renew Energy 2015;83:565–75. https://doi.org/10.1016/j.renene.2015.05.008.
[39] Visual Crossing Corporation. Visual Crossing Weather. Jan 2022 to Dec 2022, n.d, https://www.visualcrossing.com/ (accessed November 14, 2024).
[40] "Rightmove - UK's number one property website for properties for sale and to rent." Rightmove n.d, https://www.rightmove.co.uk/.
[41] Office for National Statistics (ONS), released 2 November 2022, ONS website, statistical bulletin, household and resident characteristics. vol. n.d. England and Wales: Census; 2021.
[42] CIBSE. Technical Memorandum TM59: Design methodology for the assessment of overheating risk in homes. 2017.
[43] CIBSE Guide A. Environmental design 2021. https://doi.org/10.5040/9781472596178-bed-e035.
[44] ASHRAE. ANSI/ASHRAE Standard 55: Thermal Environmental Conditions for Human Occupancy. ASHRAE Standard55; 2013. p. 76.
[45] Zimmermann J-P, Evans M, Lineham T, Griggs J, Surveys G. Harding L, et al. A Study of Domestic Electrical Product Usage: Household Electricity Survey; 2012.
[46] Palmer J, Terry N, Kane T, Firth S, Hughes M, Pope P, et al. Electrical appliances at home: Tuning in to energy savings. 2013.
[47] Chargui R, Sammouda H. Modeling of a residential house coupled with a dual source heat pump using TRNSYS software. Energy Convers Manag 2014;81: 384–99. https://doi.org/10.1016/j.enconman.2014.02.040.
[48] Aresti L, Christodoulides P, Florides G. A review of the design aspects of ground heat exchangers. Renew Sust Energ Rev 2018;92:757–73. https://doi.org/10.1016/j.rser.2018.04.053.
[49] Health and Safety Executive. Legionnaires' disease Technical guidance Part 2: The control of legionella bacteria in hot and cold water systems 2024;2002.
[50] BS EN 12897:2016. Water supply - specification for indirectly heated unvented (closed) storage water heaters (+A1:2020). 2016.
[51] Zsiborács H, Vincze A, Pintér G, Baranyai NH. The potentials of thermal energy storage using domestic electric water heater technology with PV systems in the EU countries. MRS Energy and Sustainability 2024;11:74–91. https://doi.org/10.1557/s43581-023-00072-0.
[52] Valuation office Agency. Council tax: Stock of properties 2023. GovUk. 2023.
[53] Office for National Statistics (ONS). Released 3 May 2023, ONS website, article, Insulation and energy efficiency of housing in England and Wales. 2022. n.d.
[54] Hepbasli A, Kalinci Y. A review of heat pump water heating systems. Renew Sust Energ Rev 2009;13:1211–29. https://doi.org/10.1016/j.rser.2008.08.002.
[55] Dincer I, Rosen MA. Thermal energy storage: Systems and applications. John Wiley & Sons Ltd; 2011.
[56] Xu J, Wang RZ, Li Y. A review of available technologies for seasonal thermal energy storage. Sol Energy 2014;103:610–38. https://doi.org/10.1016/j.solener.2013.06.006.
[57] Roberts BM, Abel B, Allinson D, Crowley J, Rashid T, Salehi B, et al. A dataset from synthetically occupied test houses for validating model predictions of overheating summer 2021. UK. CIBSE Tech Symp: Loughborough University; 2022.
[58] Corcoran L, Saikia P, Ugalde-Loo CE, Abeysekera M. Methodology to quantify cooling demand in typical UK dwellings. Energy Proceedings 2024:42. https://doi.org/10.46855/energy-proceedings-10996.
[59] Corcoran L, Saikia P, Ugalde-Loo CE, Abeysekera M. An effective methodology to quantify cooling demand in the UK housing stock. Appl Energy 2025;380:125002. https://doi.org/10.1016/j.apenergy.2024.125002.
[60] Saikia P, Corcoran L, Ugalde-Loo CE, Abeysekera M. A cooling demand estimator for housing communities in a warming world. Appl Energy 2025;377:124597. https://doi.org/10.1016/j.apenergy.2024.124597.
[61] United Kingdom Climate Projections (UKCP). UKCP18 n.d, https://www.metoffice.gov.uk/research/approach/collaboration/ukcp/data/index.
[62] What are El Niño and La Niña? Met Office UK 2021:1, https://www.metoffice.gov.uk/weather/learn-about/weather/oceans/el-nino#:~:text=For. example%2C El Niño years,them in our climate models.
[63] ISO 17772-1. Energy performance of buildings-Indoor environmental quality 2017: 2017.
[64] Mitchell JW, Braun JE. Design analysis and control of space conditioning equipment and systems. Solar Energy Laboratory, University of Wisconsin – Madison. 1997.
[65] Thornton JW, Bradley DE, McDowell TP, Blair NJ, Duffy MJ, LaHam ND, et al. TESSLibs 17 – Volume 11 Storage Tank Library Mathematical Reference. TRNSYS17 Documentation. 2014. p. 1–79.